Luiza Macedo

Mechanistic Modeling of Twin-Screw Powder Feeders

MASTER'S THESIS

to achieve the university degree of

Diplom-Ingenieurin

Master's degree program:

Production Science and Management

submitted to

Graz University of Technology

Supervisor

Univ.-Prof. Dr. Johannes Khinast

Institute of Process and Particle Engineering

Co-supervisor:

Dipl.-Ing. Dr. Theresa Hörmann-Kincses

Research Center Pharmaceutical Engineering GmbH

Graz, December 2020

Statutory declaration

I declare that I have authored this thesis independently, that I have not used other than the declared sources / resources, and that I have explicitly marked all material which has been quoted either literally or by content from the used sources.

Graz, 14th December 2020

Abstract

Continuous manufacturing (CM) is one of the main alternative approaches to overcome limitations of the traditional batch manufacturing in pharmaceutical production. It consists of a constant flow of material entering and exiting the process, while the process conditions are controlled through real time measurements. CM promises advantages as higher and consistent product quality, reduced costs and waste, and safer and leaner operations. However, the implementation of CM is accompanied by the challenge to add the powder shaped material at a tightly controlled rate and with constant ratios between different inlet material streams. The product specifications are critically determined by the feed rate accuracy. This work aims to develop a low-order tool for mass flow prediction during early process development, providing a better knowledge of the process, identification of critical steps and parameters that impact it the most.

In this work, mechanistic models for powder feeding process are investigated, selecting a suitable approach for the mass flow prediction. The equipment, experimental data, and different pharmaceutical powders and their properties that influence the feeding process are presented. The model chosen for the calculations is a screw conveying model based on conveying efficiency. It uses a conveying constant that allows the model to be simplified, and broadens the range in which the model can be used, permitting the analysis of new equipment and powders. For that, the powders are divided in groups related to their properties that influence the mass flow. An average of the individual conveying constants within each group is calculated, resulting in a new group constant.

Six different powders were used for the development and three for the validation of the model. Results obtained for the individual conveying constants offer a good prediction of the powder mass flow during the feeding process. However, it is observed that the model cannot predict the behavior of more compressible and electrostatically charging powders. The use of the group conveying constants for the mass flow predictions has proven to be useable too although the results are less accurate. The chosen powder densification model demonstrated good trend following for the hopper emptying experiments with declining accuracy for lower fill levels of hopper. The effects at the end of the feeding process cannot be represented by this approach. Adding further data in future could improve the predictability of the chosen models. Furthermore the more in depth studies of the powder movement inside the screw could improve the screw classification allowing for better model results.

Zusammenfassung

Kontinuierliche Herstellungsverfahren (KHV) sind eine der bedeutendsten Alternativen zur herkömmlichen chargen-weisen Produktion, um die Effizienz in der Pharma-Industrie zu steigern. Das Verfahren beruht auf konstantem Materialeintritt und -austritt in und aus dem Prozess, und der Möglichkeit Prozessbedingungen durch die Echtzeit Messungen zu kontrollieren. KHV versprechen Vorteile wie höhere und konsistentere Produktqualität, reduzierte Kosten und Abfallmengen, und einen sichereren und schlankeren Betrieb. Allerdings bringt die Einführung von KHV die große Herausforderung mit, pulverförmige Materialien in genau kontrollierten Mengen und mit konstanten Verhältnissen zwischen verschiedenen Eingangs-Materialflüssen in den Prozess zu dosieren. Die Produktqualität wird entscheidend durch die Genauigkeit der Dosierraten bestimmt. Das Ziel dieser Arbeit ist es, ein einfaches Modell für die Vorhersage der Dosierraten zu entwickeln, welches während der ersten Prozessentwicklungsphase genützt werden kann und welches besseres Prozessverständnis, sowie die Identifikation von den kritischen Prozesszonen und bedeutenden Einflussparametern ermöglicht.

In dieser Arbeit werden mechanistische Modelle betrachtet, um die an der besten geeigneten Methode für den Vorhersage der Dosierraten zu bestimmen. Das verwendete Dosierequipment, verschiedene pharmazeutische Pulver und deren prozessrelevanten Eigenschaften, sowie die experimentellen Versuchsdaten, welche zur Modellbildung verwendet werden, werden vorgestellt. Das für die Berechnungen ausgewählte Modell ist ein Schnecken-Fördermodell, welches auf einem Faktor für die Fördereffizienz (der Förderkonstante) basiert. Dieser Faktor erlaubt eine Modellvereinfachung, welche den Modelleinsatzgebiet erweitert sowie die Analyse von dem zusätzlichen Dosierern und Pulvern erlaubt. Für diesen Zweck werden die Pulver, basierend auf relevanten Eigenschaften, in Gruppen aufgeteilt. Ein Mittelwert der einzelnen Förderkonstanten wird für jede Gruppe berechnet und dann zu einer Gruppenkonstante zusammengefasst.

Es wurden insgesamt sechs Pulver für die Entwicklung und drei für die Validierung des Modells verwendet. Die für die individuellen Förderkonstanten erzielten Ergebnisse erlauben es eine gute Vorhersage der Förderraten verschiedener Pulver zu machen. Allerdings wurde beobachtet, dass das Modell bei den weniger kompressiblen sowie bei den mehr elektrostatisch aufladbaren Pulvern an Genauigkeit verliert. Der Einsatz von den Gruppenkonstanten liefert auch nutzbare Ergebnisse, jedoch ist die Genauigkeit von den Vorhersagen hier um einiges schlechter als bei den individuellen Förderkonstanten. Das gewählte Pulver Verdichtungsmodell zeigt eine gute Trendverfolgung bei den Hopper

Entleerungsversuchen, mit einer herabfallenden Genauigkeit für kleinere Füllvolumen von dem Hopper. Das Vorgehen am Ende des Entleerungsprozesses kann mit der gewählten Herangehensweise nicht modelliert werden. Das Hinzufügen von den zusätzlichen Daten würde die Vorhersagekraft von der Modellen weiter steigern. Außerdem könnten weitere Analysen von der Pulverbewegung in den Förderschnecken die Klassifizieransätze von den Dosierern verfeinern was in seiner Folge die Modellergebnisse weiter verbessern würde.

Acknowledgement

I would like to pay my special regards to my supervisor Univ.-Prof. Dr. Johannes Khinast for providing this opportunity to write my thesis in the Research Center Pharmaceutical Engineering GmbH, where I was so well supported and welcome.

My appreciation extends to my supervisor, Theresa Hörmann-Kincses, for her support and for being always available to answer my questions. I would specially like to thank and recognize Luca Orefice, whose knowledge was so invaluable for this thesis. Also, I would like to thank my colleagues, Michela Beretta and Julia Kruisz for always being available to help and to provide me with needed information.

I also thank my mother Regina and my boyfriend Pavel Butsenov whose love and support helped to keep me sane through this whole process. Without them this work would not be possible. And also thank my friends, especially Joana Pinto and Hayana Marques, who kept me going on until the end.

Contents

List of figures

List of tables

Abbreviations

AIF – Angle of internal friction, φ

API – Active pharmaceutical ingredient

AS – Auger screw

CCS – Coarse concave screw

CF – Compact Feeder 0500

CM – Continuous manufacturing

DEM – Discrete elements model

FCS – Fine concave screw

FDA – Food and Drug Administration

ffc – Flow function coefficient

FGM – Fine grade mannitol

KT20 - K-CL-KT-20

LIW – Loss-in-weight

M100 – Mannitol, gradeParteck® M 100

M200 – Mannitol, gradeParteck® M 200

MCC - Microcrystalline cellulose

MgSt – Magnesiumstearate

PAT – Process analytical technology

PH101 - Microcrystalline cellulose, grade Avicel® PH 101

PH102 - Microcrystalline cellulose, grade Avicel® PH 102

PH200 - Microcrystalline cellulose, grade Avicel® PH 200

PMIC - Paracetamol, micronized

PMIL - Paracetamol, milled

QbD – Quality-by-Design

RH - Relative humidity

WFA – Wall friction angle, Φ

List of symbols

A – Hopper cross-section

σ_v – Vertical stress

ρ_b - Bulk density

g - Gravitational acceleration

z–Distance to solids surface

dz - Height of the infinitesimal element

τ_w - Shear stress caused by the wall

C – Hopper wall perimeter

σ_h - Horizontal stress

R_H – Hydraulic radius

Φ - Wall friction angle

k – Stress ratio (Janssen coefficient)

φ - Effective angle of internal friction

a' - Coefficient from powder compressibility

b' - Coefficient from powder compressibility

h_f - Height of powder bed

μ_w - Wall friction coefficient

$\rho_{b\,min}$ - Minimum bulk density

ρ_{bmax} - Maximum bulk density

α - Powder compressibility constant

$\dot{m}$ – Mass flow

A_c – Screw conveying area cross-section

K - Conveying constant

ρ - Actual bulk density

n_s – Screw rotational speed

ε - Screw feeling degree

q – Volumetric discharge

C_s – Screw capacity

D - Outer diameter of the screw

d - Inner diameter of the screw

p - Screw pitch

t – Screw flight thickness

F_{out} - Mass flow rate

ff - Feed factor

$\rho_{effetive}$ - Density of material inside the screw pitch

V_{SP} - Volume inside the screw pitch

W - Amount of material inside the hopper

β - Exponential decay constant

H - Hausner ratio

ρ_T - Tapped bulk density

Vc - Volume of screw casing

Dc – Casing diameter

δ - Distance between the casing cylinders axes

n - Number of screw turns

V_s - Screw volume

θ–Angle of annular sector

K_{ind} - Individual conveying constant

K_{group} - Group conveying constant

1 Introduction

The quality and manufacturing of pharmaceutical products is heavily regulated, and therefore, the field of pharmaceutical production was historically not much focused on innovations. For the implementation of new technologies or operation at improved process conditions, regulatory agencies need to re-approve the manufacturing process. Thus, process conditions are typically strictly controlled after approval and the drugs are tested only at the end in batch-based operations. This testing methodology, although reliable, is very inefficient. In the case of a fault, a whole batch has to be discarded. [1][2]

The continuous manufacturing (CM) of pharmaceutical products is one of the main alternative approaches to overcome the previously mentioned limitations of traditional batch manufacturing. CM enables a deeper level of knowledge and understanding of the process[3]. The basis of this process regime is called steady state, where process control maintains the critical products attributes constant over time, promising higher product quality, higher efficiency and reduced waste[4].

However, the implementation of CM also brings some new challenges to the company, i.e., the initial effort to develop the technology, the unfamiliarity with control tools requires extra training, high initial cost, and the difficulty of producing low volume of goods[3].In addition, the biggest challenge in CM with powder raw materials is the ability to add material to the process at a tightly controlled rate and with constant ratios between different inlet material streams. The product specification, e.g., assay or content uniformity, are directly determined by the feed rate accuracy, and disturbances cause products to be out of specification. Therefore, a steady and well-controlled flow of material is a main process requirement [5]. The understanding of the interactions of powders and equipment is required to select the ideal setup and feeding strategy.

Process modeling, i.e., mechanistic modeling, has great potential to help the industry understand the process and how the variability of the material parameters influence the process performance[6].

This work aims to investigate simple mechanistic models for the two main mechanisms/zones in a powder feeder, the hopper and the twin screws. The goal was to develop a tool for mass flow prediction during early process development which additionally serves for better knowledge of the process, identification of the critical steps and the parameters that impact it the most. Initially, a review of existing modeling approaches was performed and a model structure chosen that allows to use material characterization data in combination with geometrical descriptors of the feeders to obtain

a predictive model (i.e., without feeding-experimental parameterization for each new material). Moreover, the aim was to develop a model that does not require much calculation time or large computational power. The model was then developed based on experimental feeding data of nine powders in four different feeders equipped with diverse options of twin-screws. The models rely on simplifications, yet they give a mechanistic estimation of the powder state in the feeding process. Deviations between predictions and data were then used for the refinement of the models.

2 Theoretical background

2.1 Continuous manufacturing process

The continuous manufacturing process requires a constant flow of material entering and exiting the process, while the different steps in between are sequenced to form a production line. It is often combined with in-line process analytical technology (PAT)tools, a system for analyzing and controlling the process through real time measurements [7]. The process conditions, such as temperature and concentration of components, mixing speed and others are controlled to achieve the desired product quality. In case of perturbations, small portions of non-conforming products can be disposed of without sacrificing the whole batch.

In general this lean manufacturing approach has many advantages [8] [7]:

- Safer, more efficient, and faster operations
- Lower costs and waste, more environmentally friendly
- More flexible production, easier to accommodate changes
- Faster scale up
- Safer use of hazardous reagents
- Improved quality consistency and process control

A continuous manufacturing plant being able to run constantly throughout the whole year (except in case of product change), it could easily reach a production of 1 billion tablets per year. That equals to 120 thousand tablets every hour, and this value is similar to a typical throughput of a single pilot-scale that runs with the traditional technologies. For the process that is being controlled, transient shut down – start-up operations can be minimized and controlled with accuracy, so that the products always fit the specifications. The product gets faster to the market, since the important attributes from the product can be measured during the manufacturing process and it can be distributed immediately after it is finished. CM also requires a smaller, but more skilled workforce. Nonetheless, it is a high investment to implement CM, and might be more viable for the companies to perform a lower investment only in new technologies to make a specific new product feasible. Thus, the equipment manufacturers tend to innovate more in incremental technologies than in whole new equipment trains [9].

However, the U.S.' Food and Drug Administration (FDA), as one of the biggest regulating agencies, has already acknowledged the benefits of CM and supports the industry by

encouraging a Quality-by-Design (QbD) rather that the traditional quality-by-testing approach, which can be well aligned with continuous manufacturing [10]. *Figure 1*shows an example of continuous manufacturing process, the continuous direct compression.

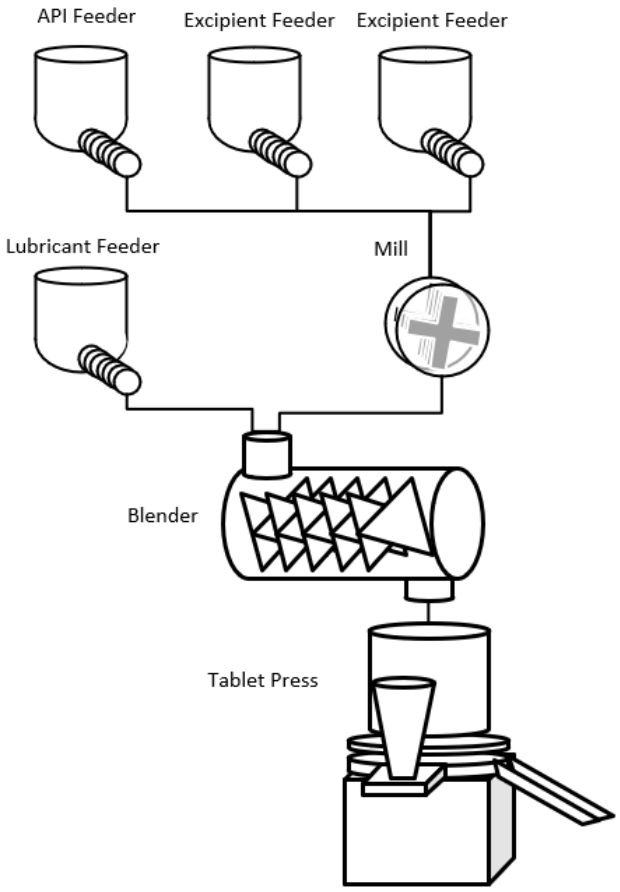

Figure 1: Continuous manufacturing process example – continuous direct compression

Every CM process starts with the feeding unit providing a steady flow of the active pharmaceutical ingredient (API) and excipients into the system and controlling the concentration of ingredients through the gravimetric feeders. If required, fed materials can be passed through a high shear mill unit, in case any lumps and agglomeration of material were present which could make the mixing of the substances more difficult. Depending on the process route used, e.g., in a continuous direct compression line, the powders are then blended to create a uniform distribution of the substances and a lubricant is added to improve flowability and facilitate the compression of the powder. After that, the material may be transferred into a tablet press or a capsule filling machine where it is compacted to tablets or dosed into capsules respectively [3].

2.2 Twin-screw feeder

Feeding is the first and most crucial operation in a CM process. Inaccurate feeding can lead to out-of-specification products since its composition is determined by the relative feed rate of the raw materials[11]. The most common type and the type used for this study are the loss-in-weight (LIW) feeders that consist of a hopper, a conveying mechanism, a gravimetric controller and a weighing platform (load cell).

The hopper is mounted on top of the weighing platform that measures the mass of the feeder together with the material stored inside. The most frequent mechanism for the control of the flow are twin screws[5]. The screws are used to displace a certain quantity of the powder based in its annular volume and rotation, maintaining steady and continuous flow. *Figure 2* illustrates an example of a twin-screw feeder. Some other mechanisms utilized to facilitate powder flow in the feeding equipment and to prevent feeding failures are vibration accessories or agitators for bridge breaking[3].To ensure reliable weight measurement in the LIW feeder, flexible connections or damping elements are used to isolate the feeding system and the weight sensing device from outside forces and vibrations [12].

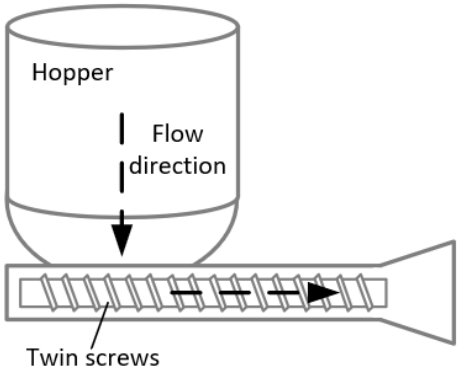

Figure 2: Twin-screw feeder illustration

The feeding operation can be realized in two different control manners, gravimetric or volumetric control.

In gravimetric control feeding, the load cell continuously measures hopper weight, and the current feed rate is determined through the weight decrease. The feed rate can be then adjusted in real time to match the set feed rate value by altering the screw rotational speed. In contrast, in volumetric control the mass flow out of the system is given by a constant screw speed, and the mass flow is merely calculated according to the rotations and the conveying volume of the screws, or calibration curve (mass flow versus screw speed). The

output is not controlled in real time, and it may vary according to the density of the material entering the screws and the degree of filling of the screw channel. For pharmaceutical applications only the gravimetric operation is used. However, during the start-up or refilling of the hopper it is not possible to operate in gravimetric mode since it is not possible to accurately measure the mass loss of the system. In this case the volumetric control is used temporarily[3].
Different indicators can be used to measure the feeding performance. Among them, the value of the maximum deviation of the flow rate, the amount of time that the flow does not correspond to the desired rate or the amount of extra raw material fed in each cycle[13]. In this work, the focus is on the mass flow range that can be achieved during feeding process. It is a useful indicator to support early process development.

Inside of the feeder hopper there are three main flow patterns that can occur: mass flow, funnel flow and expanded flow (*Figure 3*). The commonly favored one for handling of bulk materials is the mass flow pattern. In this case, the powder flows downwards at the same speed across the entire cross section of the hopper. This can be achieved, when the hopper walls in the outlet region have sufficient steepness to allow the material to slip across its surface. This flow is also characterized by first-in first-out behavior, making it the best flow pattern to handle powders that decay with time and are prone to caking. The discharge rates are more stable and the compression of the bulk solid inside the vessel can be described well. Funnel flow occurs when the walls of the hopper are not steep enough or the friction between them and the powder are enough to prevent the flow on its surface. In this pattern, a flow channel is formed above the outlet and the peripheral material stagnates. This rat-hole formation can lead to degradation or caking of the stationary material and must be avoided. The expanded flow is characterized by both occurrences simultaneously. The lower part of the hopper exhibits a mass flow pattern while in the upper part a funnel is created[14].

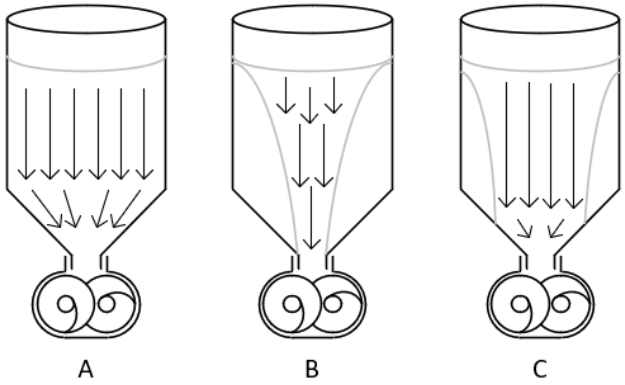

Figure 3: Flow patterns: mass flow (a), funnel flow (b) and expended flow (c)

The design of a feeder is complex and can lead to many flow problems. *Figure 4* shows images of possible failures during a feeding operation. Some of those problems are directly related to the feeder geometry and can be predicted. Others depend on many variables and the prediction is not so simple. Common flow failures include[14]:

- Bridging: A small hopper outlet causes a cohesive powder to conglomerate forming a bridge over the outlet causing the interruption of the flow.
- Rat-holing: The stagnated powder conglomerates in the periphery of the hopper and a funnel flow occurs.
- Limited discharging rate: As a powder flows through the outlet, vacuum is created above the outlet creating a counter air flow to the solids flow. In the case of the finer powders, the associated pressure might be strong enough to disturb the flow.
- Caking: After a longer storage period, some powders have the potential of gaining cohesive strength due to the undisturbed and prolonged particles interaction. The causes of the disturbance are many, like mechanical, thermal, environmental or chemical; but the most common reason is the absorption of atmospheric water [15].
- Segregation: When refilling the hopper a pile of powder is formed inside of the bin. When placed on a pile, the powders larger particles tend to roll down to the periphery of the hopper since they are free flowing; its finer particles percolate through and concentrate in the middle of the pile. So during discharge, in the occurrence of a funnel flow, the particle size distribution will not be the same as the one refilled[14].
- Tribo-charging: During the powder handling and processing, its particles collide with each other and with the equipment surface. These collisions cause an exchange

of electrons between the parts. The now electrically charged particles agglomerate in the case of different polarities and segregate when having the same charge[16].

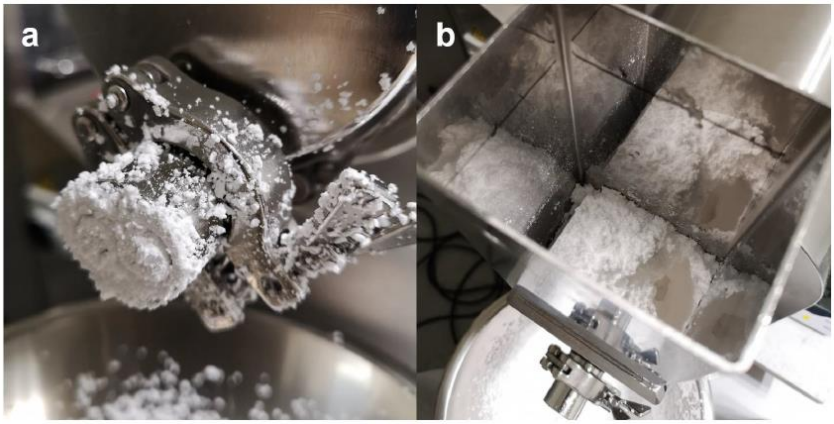

Figure 4: Failure modes: (a) electrostatic powder adhesion and (b) funnel formation [16]

2.2.1 Screw designs in twin-screws feeders

Twin-screws are commonly used in the industry as conveying elements to transport solid granular materials[17]. Regardless of the simplicity of the concept, the physics of the particles being transported inside the screw conveyor is not trivial[18]. In short, while the screw rotates in the tubular casing, a rotational movement starts in the powder due to the friction between the particles and with the screw surface. The powder flows as if undergoing small avalanches[19]. Additionally, depending on the filling level of the screw, particles can be pushed aside and remain trapped around the cylindrical wall around the screw [18].

Conveying screws have different geometries. In this study the concave screws and the auger screw are being used. *Figure 5* illustrates the two screw types.

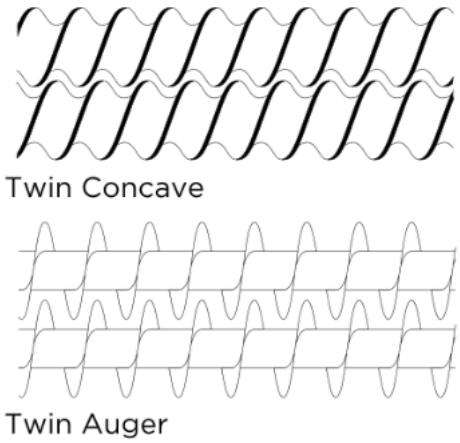

Figure 5: Screw geometries[20]

The concave screws are designed to be self-cleaning. That means that the flights of both screws are placed close to one another and remove the powder stuck to the surface. On the contrary, the auger type screws are not self-cleaning, which increases the possibility of a high cohesive material to adhere to its flights surface [21].

Figure 6: Twin-screw model: fine concave screw, coarse concave screw, fine auger screw, and coarse auger screw. [21]

The screws are also classified depending on the length of their pitch. These screw types can be seen in *Figure 6*. Screws with lower pitch length are called fine and the ones with longer length are called coarse. *Figure 7* gives details of the screws dimensions.

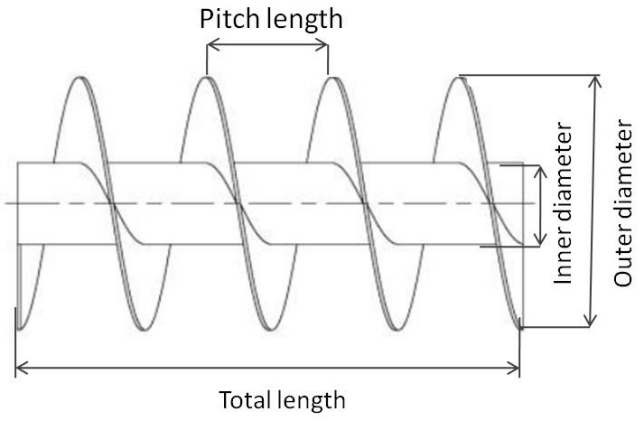

Figure 7: Screw dimensions

2.3 Models for twin-screw feeders

Different models have been developed to predict the stress distribution inside storage hoppers and work has also been done for predicting the mass flow out of feeding systems.

It is important to emphasize that due to powder characteristics, modeling such movements is quite a challenge. Granular materials can exhibit many different behaviors and the complexity of a model can easily increase. Despite of the existence of discrete element models (DEM) that are able to more precisely describe the particles interaction and behavior, they can provide limited insight for powders with more complex behavior (strong cohesive forces, non-spherical shaped particles, wall friction changes due to material deposit or electrostatic forces). The goal of this work is to make a more simplified and less time-consuming analysis by accounting for the powder bulk behavior as a continuum only, rather than a material composed of many discrete elements (no resolution of particle-particle interaction). The focus therefore lies on the accurate prediction of the average mass flow that can be achieved for a certain combination of material and feeder design.

2.3.1 Low-order twin-screw feeder modeling

The mass flow of material leaving the feeder is a key performance indicator of feeding processes and over the years, different low-order models were developed to predict this behavior. All models require an accurate estimation of the bulk state in the feeder hopper, as well as the mass of powder conveyed by a specific screw design. Thus, first a model for assessing stresses in hoppers is introduced. Next an overview of screw conveying models is given to illustrate different methods and to show their divergences and similarities. All the models, in their core, have the product of the mass of the material inside the screw and the screw rotation speed. The first two screw conveying models differ in what they are based on. The first is based on the efficiency of the conveying screws, as the second is based on the screw geometry and their filling level. The third model, being the most different of them, is a semi-empirical model highly based on experimental values.

2.3.2 Vertical stresses and bulk density in hoppers

The geometry of a hopper has major effects on the state of solids upon emptying and storage, such as the bulk density that is dependent on the pressure profile developed inside of the bin. Typically, a hopper consists of a vertical bin with a circular or square cross-section area followed by a conical or wedge-shaped outlet section. For powder feeders though, the outlet section is usually hemi-spherical or even flat, which makes the application of analytical solutions for stresses in common storage hoppers difficult.

When considering the powder bulk as a continuum, the stresses caused by the powder column in the vertical sector of the hopper increase with depth. Stresses in the vertical and

in the horizontal direction have been analyzed in [14]. Under static conditions (initial fill), lines of major stress are directed vertically. Under dynamic conditions (flow) in the bin's bottom, the major principal stress changes into the horizontal direction, as the walls converge. During the discharging of the bin, the bulk solid is compressed laterally and expands vertically. The peak stress occurs at the beginning of the converging section of the hopper [14]. These stress conditions can be seen in *Figure 8*.

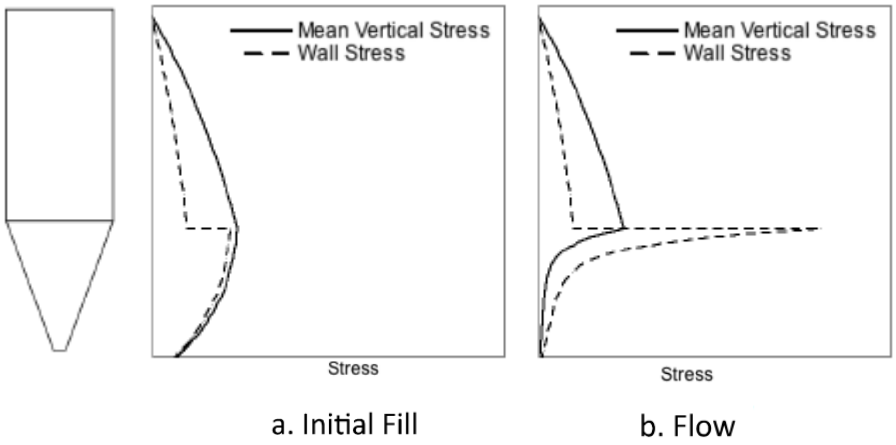

Figure 8: Stresses profiles in a hopper[14]

This continuum model-based vertical stresses model for silos was originally proposed by Janssen [et al. 1895 Janssen] and after many years his analysis is still used.

Considering a volume element with the cross-section A of the silo and an infinitesimal height, and assuming a constant vertical stress and bulk density across the area, the vertical equilibrium of forces is:

$$A\sigma_v + \rho_b g A dz = A(\sigma_v + d\sigma_v) + \tau_w C dz \quad (1)$$

where σ_v is the vertical stress, ρ_b is the bulk density of the solid, g is the gravitational acceleration,z the distance from the solids surface and dz the height of the infinitesimal element, τ_w is the shear stress caused by the wall and C its perimeter. For a better understanding, the acting forces are illustrated in *Figure 9*.

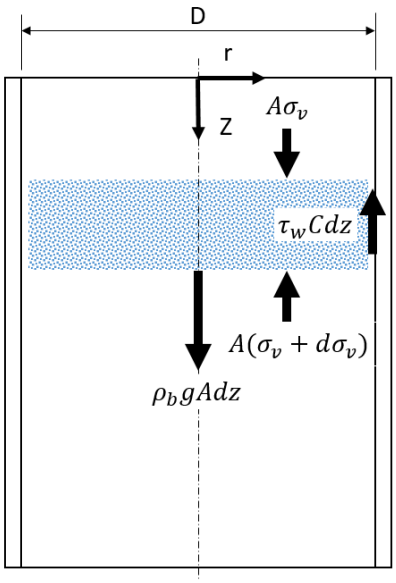

Figure 9: Stresses elements inside cylindrical hopper

Solving equation (1) leads to the vertical and horizontal stresses:

$$\sigma_v(z) = \frac{\rho_b g R_H}{k\ tan\phi'}\left[1 - exp\left(\frac{-k\ tan\Phi\ z}{R_H}\right)\right] \tag{2}$$

$$\sigma_h(z) = \frac{\rho_b g R_H}{tan\phi'}\left[1 - exp\left(\frac{-k\ tan\Phi\ z}{R_H}\right)\right] \tag{3}$$

Where the hydraulic radius R_H is given by:

$$R_H = \frac{A}{C} \tag{4}$$

And Φ is the angle of wall friction. k is the stress ratio, also known as Janssen coefficient, which is given by the ratio of the horizontal stress to the vertical stress. The k value is typically in the range of 0.3 to 0.6[14]and can be determined by:

$$k = \frac{1 - sin\varphi}{1 + sin\varphi} \tag{5}$$

where φ is the effective angle of the internal friction which is a property of the bulk solid[16].

The actual bulk density at the bottom of the hopper is a function of the stress exerted by the powder column above. In this work two models of the pressure-density correlation are presented.

The first model for the bulk density at a certain vertical stress σ_v is:

$$\rho_r(\sigma_v) = \rho_b\left(1 + \frac{a' + b'\sigma_v}{1 + b'\sigma_v}\right) \tag{6}$$

where ρ_b is the bulk density and σ_v is the pressure in the vertical direction. The coefficients a' and b'can be determined from powder compressibility test. In this model, the Janssen equation (2) is used for estimating the pressure at a certain bed depth[22]:

$$\sigma_v(h_f) = \frac{\rho_r g A}{\mu_w k C}\left[1 - exp\left(-\mu_w k h_f \frac{C}{A}\right)\right] \tag{7}$$

where μ_w is the wall friction coefficient; the k is the stress ratio already defined in equation (5) and h_f is the height of powder bed [22].

The second model estimates the density ρ_b in function of the stressσ:

$$\rho_b = \rho_{b\,min}\rho_{b\,max}\frac{1 + \alpha\sigma}{\rho_{b\,max} + \rho_{b\,min}\alpha\sigma} \tag{8}$$

σ is the resultingσ_v from the Janssen equation (2), that correlates with the consolidating pressure in the hopper geometry, at given powder properties and height of the powder column. The values of $\rho_{b\,min}$, $\rho_{b\,max}$ are reference values for the powders minimum and maximum bulk density. α is a constant related to the powder compressibility that is obtained by regressing the experimental data[14].

Using the available data the second model has proven to describe the compressibility curves better than the first. Additional benefit of the second model is its reliance on maximum and minimum bulk density, which makes it more robust for minor extrapolation around the calibrated range. Therefore, for this work the second model has been chosen.

The accuracy of this model will be analyzed in the *section 5.1.1*of this work. There the emptying process of the hopper will be modeled and compared to experimental values. For the analysis only the FGM and M200 are used, due to their difference in compressibility.

2.3.3 Screw conveying model based on screw conveying efficiency

Vetter has proposed a model to describe the feeding process [et al. 1998 Vetter]. In the work the throughput of the screw section is given by:

$$\dot{m} = A_c K n_s \rho \varepsilon \tag{9}$$

where A_c is the cross section of the total conveying area of the screw section taking in consideration the annular volume of the twin screws and the gap comprised between the screws and the screw case. K is the conveying constant that is adjusted to account for the fact that the powder in the free screw volume is not flowing all at the same speed and that not all force applied to the powder can be translated in a forward movement. Thus, these

parameter scan never reach value one for a real screw conveying process. The terms ρ andn_s are the actual bulk density and the screw rotational speed, respectively. The value εdenotes the screw filling degree. A value of one represents the case that all free volume is filled.

2.3.4 Screw conveying model based on screw fill and geometry

Another approach to calculate the throughput$\dot{m}$ of the screw feeder is:

$$\dot{m} = q.\rho_b \tag{10}$$

where q is the volumetric discharge rate and ρ_b is the bulk density.

The value of q is uniquely related to the conveying screw properties and is given by:

$$q = C_S.n_S.f \tag{11}$$

where n_S is the screw rotational speed, f is the screw filling degree.C_S is the capacity of the screw, defined by the volume comprised between the screws flights.

$$C_S = \frac{\pi}{4}(D^2 - d^2).(p - t) \tag{12}$$

where D and d are the outer and inner diameter of the screw, respectively$p$ is the screw pitch and t its flight thickness.

After calculating the screw volumetric discharge$q$, it is necessary to estimate the density of the bulk solid to calculate the mass flow$\dot{m}$. The density in function of the hopper level can be calculated using one of the models presented previously in section 2.3.2.

2.3.5 Semi-empirical model

Alternatively, a semi-empirical model is illustrated that can be used to simulate the LIW feeding behavior based on experimental data. The mass flowrate as a function of time is given by the expression:

$$F_{out}(t) = ff(t).n_S(t) \tag{13}$$

where $n_S(t)$ is the screw speed and $ff(t)$ is the feed factor that is defined as the maximum mass of the bulk solid that can be conveyed in the screw flights.

$$ff(t) = \rho_{effetive}(t).V_{SP} \tag{14}$$

where $\rho_{effective}(t)$ is the density of the material inside the screw pitch, which is also related to the filling degree of the screw. V_{SP} is the volume of the screw pitch. The effective density and in consequence the feed factor is dependent on the amount of material inside the hopper, represented by $W(t)$. This connection is defined in:

$$ff(W(t)) = ff_{level}^{sat} - exp[-\beta W(t)]\left(ff_{level}^{sat} - ff_{level}^{min}\right) \quad (15)$$

The saturated feed factor, the minimum feed factor and the exponential decay constant β are coefficients related to the material propertiesand feeder geometry, being regressed from experimental feeding data[23].

The model chosen for this study was the screw conveying model based on screw conveying efficiency. It was chosen because it is a simple classical model, and the use of the conveying constant K allows useful simplifications. The conveying constant K can be determined for each powder, feeder and screw combination using mass flow values obtained in previous experiments. These powders then are separated into groups for which only one value of K is defined. This group K simplification allows using the model to predict the mass flow of new powders or powder-feeder-screw combinations not tested in past experiments. To validate the mass flow model, experimental values were compared to predictions of the powders used in the dataset. Furthermore, prediction values for the additional powders not used in the model dataset were calculated. The data for these powders was obtained under different experimental conditions and batches of raw material, therefore not suitable as model dataset. However, still useful for comparing the accuracy of the group predictions.

2.4 Pharmaceutical powders and their properties

In the pharmaceutical industry, most of the raw material processed is in the form of powders with small grain sizes. Modeling powder state, in general, is quite a unique challenge, since they can show a broad range of behaviors, acting similar to solids, liquids or gases, depending on their dilution/densification state. [24].

In contrast to liquids, the movement of powders depends on many intrinsic physical properties (size, shape), bulk properties (bulk density, cohesion), external factors (temperature and humidity) and the processing conditions (compression). Depending on the process parameters the powders are subjected to many different conditions, therefore an extensive characterization is needed to understand their behavior during the manufacturing process.[25]

The following chapter gives a brief explanation of the macroscopic powder properties that are relevant for the previously introduced models.

2.4.1 Powder bulk properties

2.4.1.1 Bulk density

The ratio between the mass and the volume occupied by a powder is called bulk density. It can vary greatly depending on the manner that the grains are packed, therefore in contrast to liquids or solids it is not a single value.

Some methods to determinate bulk density of a powder, related to its packing are:

- The poured bulk density is determined by pouring the material and allowing it to settle under influence of gravity only. A bulk solid with a high structural strength will settle and resist collapse. Therefore it will have a low bulk density. However, a weak structured powder will collapse easier and have a higher bulk density.
- The tapped bulk density is determined after the tapping of the container that holds the bulk solid. With the tapping, a cohesive powder structure will collapse and densify further, while a free-flowing powder structure does not have much more space for further rearrangement for denser packing.

The ratio between the bulk density and the tapped bulk density is called the Hausner ratio. Used in diverse types of industry, it is one of the most common indicator of cohesion of a material and its flowability[26].

$$H = \frac{\rho_B}{\rho_T} \tag{16}$$

Lower values of the Hausner ratio indicate powders with excellent flowability, higher values are indicative of very poor flowability*(Table 2.1)*[27].

Table 2.1: Classification of powder flow by the Hausner ratio value [27].

Flow nature	Hausner Ratio
Excellent flow	1,00 – 1,11
Good flow	1,12 – 1,18
Fair flow	1,19 – 1,25
Passable	1,26 – 1,34
Poor flow	1,35 – 1,45
Very poor flow	1,46 – 1,59
Extremely poor flow	>1,60

2.4.1.2 Compressibility

Compressibility is the ability of a material to reduce its volume under pressure, i.e. under stress. This pressure-volume connection can be measured in experiments, and is affected by numerous factors such as e.g., moisture, particle size and shape, temperature, and particle elasticity. High moisture and higher temperatures make the material more

compressible, the shape defines how the particles fit together and higher elastic values of particles lead to bigger deformations when compressed[27].

Inside the feeder, the compressibility is a crucial property to correlate the stresses within the powder bed and the actual bulk density of the powder flowing into the twin-screws.

There are models developed to study this relationship between the density and the pressure caused by the powder bed inside of a hopper cylinder. Two models were already discussed previously in the section 2.3.2.

2.4.1.3 Powder rheology

The flowability of a powder is commonly described by the flow function coefficient (ffc). The ffc is defined by the ratio between the major principal stress and the unconfined yield strength, that are obtained through the shear cell test [16].

$$ffc = \frac{\sigma_1}{\sigma_c} \tag{17}$$

A shear cell test permits powders to be compressed and sheared under controlled stress conditions. It generates pairs of values for normal load and shear force where the powder starts to flow. Plotting these value pairs gives the yield locus for a specific powder in a specific compression state (*Figure 10*). Two tangential Mohr's circles are interesting for the analysis, the smaller Mohr's circle represents the unconfined conditions, and the larger Mohr's circle represents the conditions at steady state shear flow. When combining several yield loci determined at different consolidation states, the effective yield locus, describing powder behavior across a wide range of conditions can be obtained. [28]

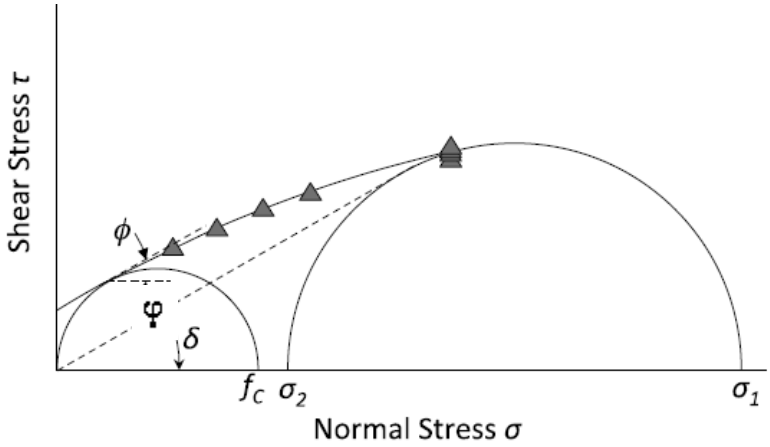

Figure 10: Yield locus[14].

According to the ffc value, materials can be categorized in different groups[16]as it is shown in *Table 2.2*.

Table 2.2: Classification of powder flowability by the ffc value[29].

Flowability	ffc
Not flowing	<1
Very cohesive	1 – 2
Cohesive	2 – 4
Easy flowing	4 – 10
Free flowing	>10

2.4.1.4 Effective angle of internal friction

The angle of internal friction (φ) is an indicator of the internal friction in a bulk material upon onset of shear and is derived from the shear cell test. The effective φ is determined through the yield locus. A line from the origin, being tangent to the larger Mohr's circle is drawn and the angle formed represents the effective angle of internal friction[14].

The φ value is associated to stress ratio k (equation (5)), which is the ratio of the vertical and horizontal stress inside of the hopper.

2.4.1.5 Wall friction

The wall friction angle (Φ) is the measure of the sliding friction at the interface between the powder and a wall (e.g., hopper wall) [30]. It is experimentally determined by shearing the powder against a sample of the wall material under different normal stresses. Apart from the powder properties, the value depends on the wall roughness and the environmental relative humidity (RH) during the experiment [16].

Φ has a direct impact on the flow pattern inside of the hopper and is used in the consolidation pressure calculation. The application of vibration could reduce its value and change the pattern from a funnel flow to a mass flow. [31].

3 Materials and methods

3.1 Pharmaceutical powders

Data from six different powders were used to build the model in this study and three were used for validation. Among them, APIs, excipients, and a lubricant. The following *Table 3.1*provides an overview of the materials.

Table 3.1: Material overview

Abbreviation	Material Type	Grade	Manufacturer	Use
PH200	MCC	Avicel® PH 200	DuPont, USA	Dataset
PH102	MCC	Avicel® PH 102	DuPont, USA	Validation
PH101	MCC	Avicel® PH 101	DuPont, USA	Dataset
PMIC	Paracetamol	Fine micronized	Mallinckrodt, Ireland	Dataset
PMIL	Paracetamol	Fine milled	Mallinckrodt, Ireland	Validation
MgSt	Magnesium Stearate	Parteck® LUB MgSt-V	Merck, Germany	Dataset
M200	Mannitol	Parteck® M 200	Merck, Germany	Dataset
M100	Mannitol	Parteck® M 100	Merck, Germany	Validation
FGM	Mannitol	Fine Grade	Merck, Germany	Dataset

3.1.1 Microcrystalline cellulose

Microcrystalline cellulose (MCC) is a widely used material as excipient for direct compression formulations. An excipient is added tot he product due to its functionality to improve the manufacture or the quality of the product.

MCC is a free-flowing bulk solid offered in different grain sizes*(Figure 11)*.The grades used for this study are the PH200, PH102 and PH101, in which the numbers signify different particle size distribution. They are materials with low bulk density and low compressibility index. Coarser versions of MCC, as PH200, have a better flowability than the finer versions (PH101)[32].

Figure 11: MCC particle shape and size distribution for different grades[33]

3.1.2 Paracetamol

Paracetamol is one of the most frequently used antipyretic and analgesic API in the world[34]. For this study two types of paracetamol are used: PMIL and PMIC. PMIL is produced by conventional milling, on the other hand PMIC is produced by micronization, yielding very small particles [35].

3.1.3 Magnesium Stearate

Magnesium stearate (MgSt) as lubricants plays an important role for achieving success in the CM process. During blending, tableting or capsule filling, a lubricant is used to reduce the friction between the solid material and the equipment surfaces. Thus, they increase the flowability and reduce adhesion of the processed materials [36]. It is the most compressible powder used in this study, therefore the consolidation pressure is expected to have the biggest influence.

3.1.4 Mannitol

Mannitol, which is usually manufactured from fructose, is a sugar alcohol used as an excipient in the manufacture of capsules and tablets. Being sweet and odorless, it also can be used as sweetener and food additive in the food industry[37].

In this study three different grades of mannitol were used. M200 and M100 are manufactured by spray drying and agglomeration, while FGM is produced via crystallization, which results in smaller particles, therefore showing higher cohesivity [14].

3.2 Powders properties

Most important powder properties used for the mass flow calculations in the low-order feeding model for each material are presented below *(Table 3.2, Table 3.3)*.

These values were obtained in experiments done previously, and they were obtained using a FT4 powder rheometer (Freeman Technologies, USA) to perform the shear cell, compressibility, and wall friction analysis. Measurements were performed in triplicates, and shear cell tests performed with a pre-shear stress of 3kPa.

For the WFA, the experiment was done with a 0.28 μm roughness stainless steel plate.

The compressibility tests were performed at the normal stress increasing from 0.5 kPa to 15 kPa.

Table 3.2: Powders properties data

Powder	Bulk Density [g/cm^3]	Φ [°]	ffc	φ [°]	x50 [μm]
PH200	0.350	6.83	100	28.13	244.12
PH102	0.359	9.77	16.8	32.23	129.56
PH101	0.336	10.43	9.89	40.47	99.67
PMIC	0.230	12.17	1.57	55.23	8.03
PMIL	0.216	13.57	2.38	48.53	18.63
MgSt	0.204	7.00	3.17	35.5	5.61
M200	0.514	13.57	100	32.07	147.81
M100	0.608	13.13	45.00	30.87	106.95
FGM	0.590	17.2	2.30	48.67	33.86

Table 3.3: Powder compressibility data

Powder	ϱ 0.5kPa	ϱ 1kPa	ϱ 2kPa	ϱ 4kPa	ϱ 6kPa	ϱ 8kPa	ϱ 10kPa	ϱ 12kPa	ϱ 15kPa
PH200	0.5275	0.53	0.5335	0.5375	0.54	0.542	0.544	0.546	0.548
PH102	0.3667	0.372	0.379	0.3857	0.39	0.3933	0.3957	0.398	0.4003
PH101	0.5147	0.523	0.5347	0.5473	0.5553	0.561	0.565	0.569	0.5743
PMIC	0.2447	0.2627	0.2847	0.312	0.3287	0.342	0.3523	0.361	0.3727
PMIL	0.2627	0.2873	0.319	0.354	0.3753	0.3923	0.4063	0.4177	0.4323
MgSt	0.3347	0.3603	0.3893	0.4183	0.4353	0.4487	0.4593	0.4673	0.4773
M200	0.5477	0.5497	0.5527	0.5557	0.5577	0.5597	0.56133	0.563	0.565
M100	0.6203	0.6237	0.62833	0.63233	0.6343	0.6363	0.638	0.6397	0.642
FGM	0.5607	0.5777	0.6083	0.6507	0.676	0.693	0.7067	0.718	0.736

3.3 Feeders

The feeding model was developed for four models of LIW feeders.

- The Compact Feeder 0500 (GEA Pharma, Belgium) (CF500) is a pilot-scale flat bottom feeder*(Figure 12d)*. Feeding experiments were made with fine concave screw (FCS), coarse concave screw (CCS), and auger screw (AS).Additionally, the experimental data is available for two different options of the vertically mounted agitator for the CF500, changing the height of where it breaks the bridges. In the model it is considered as a different feeder called CF500_GB2 adapted hopper.

- The K-CL-KT-20 (Coperion-KTron, Switzerland) (KT20) is a pilot-scale rounded bottom feeder with a horizontal two-bladed agitator mounted above the twin-screws. The previous experiments were performed with the AS, FCS and CCS*(Figure 12a)*.
- MT-SHyg (Brabender Technologie, Germany), as a small-scale feeder has a rectangular cross-section hopper and is curved in the bottom*(Figure 12b).*A 2-bladed agitator is mounted horizontally above the twin-screws. Experimental data is available for CCS and FCS.
- The ZD-12 FB (ThreeTec, Switzerland) is a small-scale feeder with cylindrical, flat bottom hopper and a vertical bottom mounted agitator. Feeding experiments were realized with CCS *(Figure 12c)*.

Table 3.4: Feeder data

	KT20	**CF500**	**CF500 ad. hopper**	**ZD-12**	**MT-S Hyg**
Screw speed max [rpm]	154	124	124	270	140
Hopper volume [L]	10.5	2.3	2.3	0.96	1.33
Hopper fill level [mm]	301	130	130	121	240.5
Diameter hopper [mm]	220	150	150	100.4	65

Figure 12: Used feeder model: (a) KT-20, (b)MT-S Hyg , (c)ZD-12 FB and (d)CF500.

3.4 Screw designs

The model was developed based on data from different combination of feeders and twin-screw types.

The mass flow out of the system is related to the amount of powder that fits in the screw, which is connected to the conveying volume. The conveying volume available in the screw was calculated considering the total volume inside of the casing and then subtracting the volume of the screw itself.

The cross-section area of the casing has the shape of two intersecting cylinders, as shown in *Figure 13*.

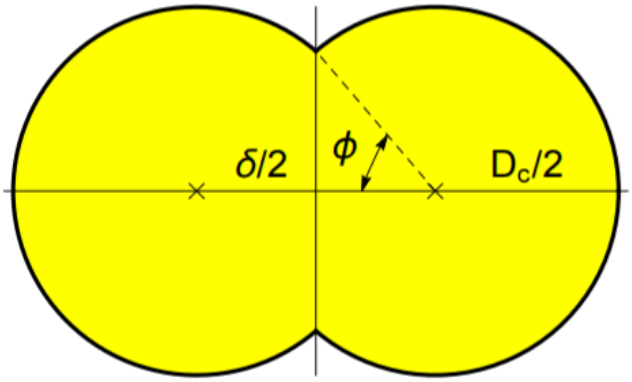

Figure 13: Screw casing cross-section area

The volume of the case is calculated by:

$$Vc = \frac{Dc^2}{2}\left[\pi - arccos\left(\frac{\delta}{D_c}\right) + \frac{\delta}{D_c}\sqrt{1-\left(\frac{\delta}{D_c}\right)^2}\right]np \tag{18}$$

where D_c is the casing diameter, δ is the distance between the axes of the two cylinders, n and p are the number of screw turns and the pitch length, respectively.

The screw volume calculation is different for the two screws geometries, since their flight shapes are not the same.

For the auger screw, the volume is defined by the sum of the shaft volume and the flights volume.

$$V_s = \frac{1}{4}\left[\pi d^2 + \frac{\theta(t)}{2}(D^2 - d^2)\right]np \tag{19}$$

Where d is the diameter of the screw shaft and the D the outer diameter of the screw blades *(Figure 14)*. $\theta(t)$ is the angle of the annular sector, and it's a function of the flight thickness given by the equation (20).

$$\theta = \frac{2t\sqrt{(\pi(D+d))^2 + p^2}}{(D+d)p} \tag{20}$$

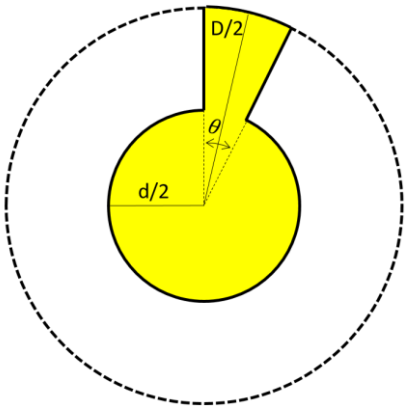

Figure 14: Screw diameters and angle of annular sector

For the concave screws, independently of coarse or fine, the cross-section is calculated as the intersection of two circles of radius R centered in ±(R-δ) and given by the equation (21).

$$V_S = \frac{D^2}{4}\left[\frac{(D^2+d^2)^2}{2D^2d^2}\phi - \frac{2}{\tan(\phi)}\right]np \tag{21}$$

The value of $\tan(\phi)$ and consequently ϕ is given by the formula:

$$\tan(\phi) = \frac{2Dd}{D^2 - d^2} \tag{22}$$

The calculations were performed for all the screws used in the study. Following is the measured data used for the calculations (*Table 3.5*) and the results (*Table 3.6*).

Table 3.5: Measured screw design data.

	KT20		CF500			ZD-12	MT-S Hyg	
	AS	CCS	AS	CCS	FCS	CCS	CCS	FCS
d [mm]	13	14.5	13.1	13.3	13.3	7.7	9	9.5
D [mm]	20.5	18.5	19.7	19.8	19.7	12	11.5	11.5
p [mm]	26	20	20	20	10	18	13	4.5
n [-]	9.6	12.5	18.5	18.5	37	12.5	8.5	9.1
D_c [mm]	22	22	21.3	21.3	21.3	13.7	12.95	12.95
δ_c[mm]	17	17	17	17	17	10.4	11	11

Table 3.6: Calculated screws conveying volume

	KT20		CF500			ZD-12	MT-S Hyg	
	AS	CCS	AS	CCS	FCS	CCS	CCS	FCS
Screwconveying volume no gap [cm³]	88.64	132.56	113.99	220.73	218.83	49.44	22.29	8.46
Gap volume [cm³]	19.88	45.57	30.94	29.03	30.94	12.36	5.16	1.96
Total conveying volume gap [cm³]	108.52	178.14	144.93	249.77	249.77	61.80	27.45	10.42

The annular volume of the screw and the volume comprised between the screw and the case were kept separated. In the model, it is possible to select the degree of the powder adhesion in the case wall in percentage, to analyze its influence on the results.

3.5 Mass flow experimental data

Feeding experiments were executed in volumetric feeding mode for all available setups. A reference catch-scale (SW 1000/1000-FS, Wipotec, Germany) was used in all tests to determine the mass flow rate of all feeders in a comparable way. Data from this catch-scale was collected via a data acquisition software (XAMControl, evon-Automation, Austria) every 400 ms. MATLAB® (MathWorks, USA) was used to derive the mass flow data from the weight gain data on the catch scale. A forward-backward (zero phase) moving average filter with 10 s span was used to achieve a good signal-to-noise ratio in the mass flow data.

Data from two different tests was used for the model development in this thesis: i) the mass flow rate screening test and ii) the hopper emptying test. In the mass flow rate screening test, constant screw speed levels (20, 50, 80% of max. screw speed) was set for

every feeder and the dosed mass collected on the catch-scale for 5 min. The hopper fill level was always kept at 90-100% fill level during the experiments to ensure constant densification of the powder. The average mass flow was then calculated for each screw speed level. The results of the mass flow test can be seen in the Appendix section *7.1* in the *Table 7.1*. For hopper emptying runs, the feeder was filled completely (to 100% fill level) and then emptied at a constant screw speed (50% of max. speed). Throughout the entire run, material was collected on the catch-scale and the collection bowl changed when full. The data during the bowl-exchanges was cut from the final mass flow data set and replaced by NaN to avoid falsification of feeding statistics. The mass flow data over time or fill level was then evaluated as response of this feeding test.

4 Model development

4.1 Model parameterization work flow

The mass flow prediction model that was chosen is the screw conveying model based on screw conveying efficiency. The choice was motivated by its use of a conveying constant, which allows simplifications of the model. This enables the expansion of the mass flow prediction range to different combinations of screws, feeders and powders not analyzed in experiments and allows adding the new powders.

A small change in the formula (9)was made. In order to make the conveying constant K adimensional, the terms would be multiplied by the screw conveying volume instead of the screw conveying area, resulting in the new equation:

$$\dot{m} = VKn_s\rho\varepsilon \tag{23}$$

Moreover, the following assumptions were made during model development:

- The screw filling degree ε is assumed to have a unitary value, symbolizing that the screw is always full.
- The screw conveying area A_c is the sum of the conveying area inside of the screw and the space between the screw and the screw casing wall. This area close to the casing, in the model, can be multiplied by a rate that symbolizes the adhesion of the powder on the wall. The unitary value means that all powder comprised in this area can move freely, and a null value means that all the area is completely filled with stagnated material.

The preferred stress-density model for determining the bulk density inside of the hopper was the defined by equation (8). In this, values for maximum and minimum bulk density, as well as a densification constant α are used.

4.1.1 *Consolidation pressure and bulk density*

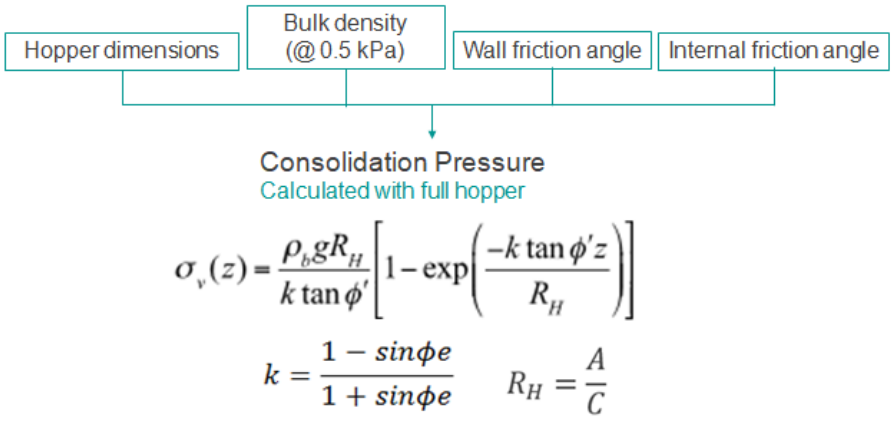

Figure 15: Hopper stress calculation work flow.

The first step is the estimation of the consolidation pressure at the feeder bottom, considering the hopper completely filled. It is calculated for each powder-feeder combination.

The consolidation stress inside of the feeder is calculated with formula (2), and the equation is dependable of the bulk density of the raw material stored inside the hopper. However, the actual bulk density of the material given by the equation (8) is dependable of the consolidation stress caused by the powder inside the hopper. Therefore, the bulk density value used in equation (2) was considered to be the density at a 0.5kPa obtained experimentally by the compressibility test. The compressibility data for each powder is presented in *Table* 3.3. For a better understanding, a work flow is presented at *Figure 15*.

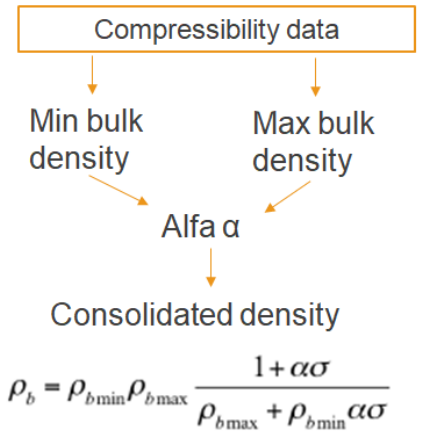

Figure 16: Bulk density model fitting

After the consolidation stress was determined, the powders actual bulk density at the bottom of the hopper is calculated using the formula (8), as shown in *Figure 16*.

Initially, the terms of the equation for each powder must be defined. The constant α, and the values for ρ_{bmin} and $\rho_{b\ max}$ are defined through a curve fitting method. The calculation starts with initial values for the three terms, and a transitory value of bulk density is calculated for each consolidation stress value. The values are then compared to the experimental values from the compressibility test, and their difference is calculated. With the use of the GRG nonlinear solver algorithm in Excel, final values for ρ_{bmin} and $\rho_{b\ max}$ are obtained by minimizing the difference between the calculated and the experimental values. The *Table 4.1* presents the result for the fitting values for each powder. The calculation and the graphs with the curve fitting results can be found in the Appendix, section *7.2*.

Table 4.1: Alfa, minimum and maximum density results

Material	Alfa	Max bulk density [g/cm³]	Min bulk density [g/cm³]
M100	0.2379	0.6476	0.6180
M200	0.1122	0.5756	0.5468
FGM	0.2566	0.8078	0.5394
PH102	0.2851	0.4096	0.3620
PH200	0.1387	0.5585	0.5261
PH101	0.2605	0.5925	0.5070
MgSt	0.4717	0.5110	0.3130
PMIC	0.3336	0.4202	0.2314
PMIL	0.4050	0.4893	0.2439

4.1.2 Determination of the conveying constant K

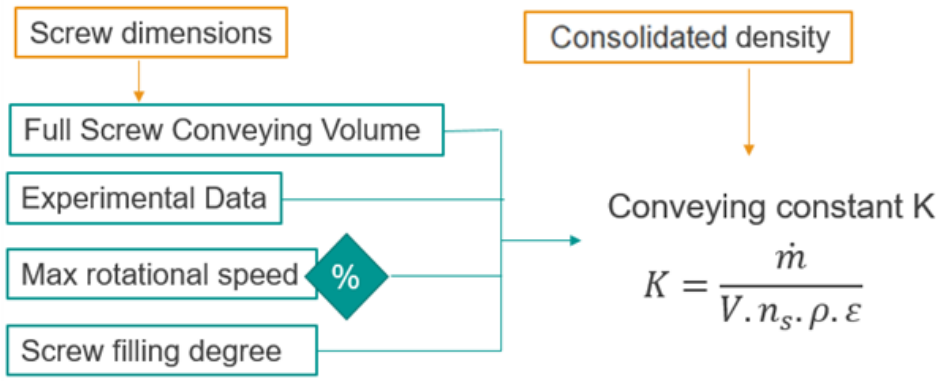

Figure 17: Conveying efficiency constant fitting

Once the consolidated bulk density and screw geometry are defined, together with the mass flow experimental data, the conveying constant K can be determined (*Figure 17*). The formula (23) is rearranged, to isolate the constant:

$$K = \frac{\dot{m}}{V n_s \rho \varepsilon} \tag{24}$$

The value of the constant$K$ is obtained for each powder, feeder and screw combination for the screw rotational speed of 20%, 50% and 80% of its maximum value. The mass flow values were obtained in previous experiments and they are presented in the Appendix, section*7.1*. For each powder-screw-feeder setup, the average Kacross the different rotational screw speeds was calculated to obtain the individual K_{ind} of each combination. In the Kdefinition calculations, the value of the screw conveying volume also includes the gap between the screw and the screw casing. The density is considered to be the actual bulk density with a full hopper. The *Table 4.2* presents the results for K for each setup and for the different screw rotation speed, and additionally their average K_{ind} value.

Table 4.2: Individual K results

Feeder	Material	Screw	K_20	K_50	K_80	K_{ind}
CF0500_GB2	FGM	'AS'	0.0190	0.0194	0.0180	0.0188
CF0500_GB2	M200	'AS'	0.0177	0.0161	0.0156	0.0165
CF0500_GB2	PH101	'AS'	0.0137	0.0140	0.0143	0.0140
CF0500_GB2	PMIC	'AS'	0.0009	0.0003	0.0023	0.0012
CF0500_GB2	PH200	'AS'	0.0154	0.0158	0.0151	0.0154
CF0500_GB2	PH101	'CCS'	0.0093	0.0101	0.0099	0.0098
CF0500_GB2	FGM	'CCS'	0.0132	0.0133	0.0122	0.0129
CF0500_GB2	M200	'CCS'	0.0125	0.0118	0.0112	0.0118
CF0500_GB2	PMIC	'CCS'	0.0022	0.0021	0.0024	0.0022
CF0500_GB2	PH200	'CCS'	0.0120	0.0113	0.0161	0.0131
CF0500_GB2	PH101	'FCS'	0.0043	0.0050	0.0052	0.0048
CF0500_GB2	PMIC	'FCS'	0.0008	0.0005	0.0009	0.0008
CF0500_GB2	FGM	'FCS'	0.0060	0.0041	0.0035	0.0045
CF0500_GB2	M200	'FCS'	0.0050	0.0047	0.0034	0.0044
CF0500_GB2	PH200	'FCS'	0.0058	0.0056	0.0062	0.0058
CF0500_GB2_adhopper	PH101	'CCS'	0.0106	0.0108	0.0109	0.0109
CF0500_GB2_adhopper	FGM	'CCS'	0.0166	0.0134	0.0162	0.0154
CF0500_GB2_adhopper	M200	'CCS'	0.0149	0.0145	0.0136	0.0143
CF0500_GB2_adhopper	PMIC	'CCS'	0.0029	0.0028	0.0025	0.0028
CF0500_GB2_adhopper	PH200	'CCS'	0.0115	0.0115	0.0116	0.0115
K-CL-KT20	PH101	'AS'	0.0261	0.0262	0.0276	0.0266

Feeder	Material	Screw	K_20	K_50	K_80	K_{ind}
K-CL-KT20	PMIC	'AS'	0.0108	0.0110	0.0108	0.0109
K-CL-KT20	FGM	'AS'	0.0346	0.0311	0.0301	0.0319
K-CL-KT20	M200	'AS'	0.0503	0.0484	0.0469	0.0485
K-CL-KT20	PH200	'AS'	0.0347	0.0331	0.0341	0.0340
K-CL-KT20	PH101	'CCS'	0.0183	0.0174	0.0155	0.0171
K-CL-KT20	PMIC	'CCS'	0.0073	0.0074	0.0084	0.0077
K-CL-KT20	FGM	'CCS'	0.0254	0.0238	0.0270	0.0254
K-CL-KT20	M200	'CCS'	0.0258	0.0265	0.0251	0.0258
K-CL-KT20	PH200	'CCS'	0.0149	0.0149	0.0156	0.0151
MT-S Hyg	FGM	'CCS'	0.0068	0.0046	0.0036	0.0050
MT-S Hyg	M200	'CCS'	0.0183	0.0183	0.0181	0.0182
MT-S Hyg	PH101	'CCS'	0.0105	0.0107	0.0109	0.0107
MT-S Hyg	PH200	'CCS'	0.0116	0.0119	0.0123	0.0119
MT-S Hyg	FGM	'FCS'	0.0076	0.0060	0.0047	0.0061
MT-S Hyg	M200	'FCS'	0.0221	0.0227	0.0217	0.0221
ZD-12 FB	PH101	'CCS'	0.0096	0.0101	0.0114	0.0104
ZD-12 FB	MgSt	'CCS'	0.0105	0.0110	0.0119	0.0111
ZD-12 FB	FGM	'CCS'	0.0108	0.0117	0.0106	0.0110
ZD-12 FB	M200	'CCS'	0.0165	0.0182	0.0177	0.0175
ZD-12 FB	PMIC	'CCS'	0.0009	0.0005	0.0005	0.0006
ZD-12 FB	PH200	'CCS'	0.0110	0.0118	0.0123	0.0117

The value of$\boldsymbol{K_{ind}}$is only used to calculate the mass flow for the feeder-powder-screw combinations that they originate from. Therefore, different ways of grouping these $\boldsymbol{K_{ind}}$ values are discussed in the next section in order to achieve predictability for other combinations that were not studied in the previous experiments.

4.1.3 Classification of the conveying constant K per material groups and screws

Nine powders were used for the development and verification of this model. Among those, six were used for the model dataset (PMIC, FGM, MgSt, PH101, PH200 and M200) and the other three were added to the model later for verification (PMIL, PH102 and M100).The nine powders were arranged in groups following five different classifications. These groups are based in the powder characteristics that could influence the mass flow. The classifications can be seen further on in *Table 4.3* to Table 4.7.

- Flowability: it is a direct indicator of the ability of the powder to flow.

Table 4.3: Flowability K classification

	PMIC	PMIL	FGM	MgSt	PH101	PH102	M100	PH200	M200
ffc	1.167	1.707	2.097	4.08	5.39	17.867	40.933	47.2667	79

- Material substance group: the powders were grouped according to their types, taking into consideration that same group powders have similar properties.

Table 4.4: Material substance K classification

	FGM	M100	M200	MgSt	PH101	PH102	PH200	PMIC	PMIL
Material substance	Mannitol				Avicel			Paracetamol	

- Particle size: it has a great influence on how the particles flow out of the hopper, being an easily measurable parameter.

Table 4.5: Particle size K classification

	PMIC	MgSt	PMIL	FGM	PH101	M100	PH102	M200	PH200
Size (x50)	6.897	7.01	18.843	25.85	99.67	102.14	129.56	149.85	244.12

- WFA: it has a direct impact on the type of flow that occurs inside of the hopper and on the stagnation of materials on the hopper walls.

Table 4.6: Wall friction angle K classification

	PH102	PH200	M100	PH101	M200	PMIC	MgSt	FGM	PMIL
WFA	5.69	5.883	7.937	8.843	8.963	9.467	9.717	12.067	12.767

- Statistical model: a principal component analysis (PCA, in SIMCA 16, Umetrics, Sweden) was performed to identify similarities and dissimilarities between the materials and to analyze correlations between the material properties. It was built taking into consideration

several material attributes as shown in *Figure 18*, e.g.: specific surface area (SSA), cohesion (C), WFA, AIF, compressibility (CPL).

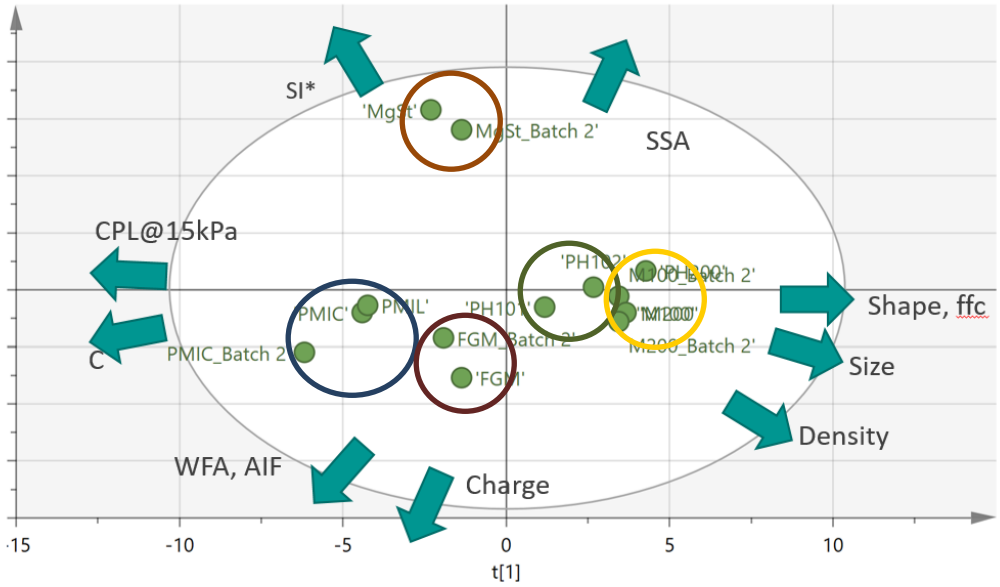

Figure 18: Statistical model materials attribute influences

Table 4.7: Statistic model K classification

Stat model	PMIC	PMIL	FGM	MgSt	PH101	PH102	M100	PH200	M200

The different powder classifications were considered for comparison combined with the screw type. The square sum of error of all the K_{ind} inside of the classification to the new grouped value was calculated and summed to analyze which of the groups has the smallest divergence. A ranking (*Table 4.8*) was created to define which group has the better fit as an approximation.

Table 4.8: Groups classification ranking

Classification	$\sum(K_{group} - K_{ind})^2$
Stat Model + Screw	0.001544618
ffc + Screw	0.001620648
Material substance + Screw	0.001645068
Size + Screw	0.002261405
WFA + Screw	0.002416555

According the table above, the statistical model and the flowability group classifications are the ones that have the best fit to the individual K_{ind}. Therefore in our model we are going to use the statistical model+screw and the ffc+screw classification for the groups mass flow prediction.

4.1.3.1 Influences on the K value

For the K calculations, some assumptions regarding the screw conveying volume and the density were made. To measure the influence of the assumptions, the values of the K_{ind} for different scenarios were analyzed.

The fist analysis compared the difference in the K_{ind} value to the values considering a scenario in that the conveying volume does not include the gap comprised between the twin-screws and the screw case. The new K_{ind} values without the gap have an increment of 14% to 27% and can be seen in the*Table 7.2* in the *Appendix, section 7*. However this effect is compensated by choosing the corresponding value for the cross section parameter in mass flow calculation (equation (9)).

The influence of the bulk density values was also analyzed. The bulk density value used in equation (2) to determine the consolidation pressure that will be used for the K calculation (*section 4.1.1*) was changed from the 0.5 kPa compressibility test bulk density to the bulk density result from the poured bulk density tests. The divergence calculated was of less than 10% for the most compressible powders and of 40% to less compressible powders. These values could be explained by the fact that for the less compressible powders the poured bulk density is much smaller than the 0.5 kPa bulk density, and the latest is much closer to the density value inside a full hopper. Therefore, using the poured bulk density for the K determination results in a much larger value for the K. The results values are found in the *Table 7.3* in the Appendix, section 7.3.

4.2 Mass flow prediction work flow

The grouped values of K, the screw data and the actual density of the raw material density are input to equation (23)for the prediction of mass flow. In *Figure 19* the mass flow prediction workflow is shown, for a better understanding of the process.

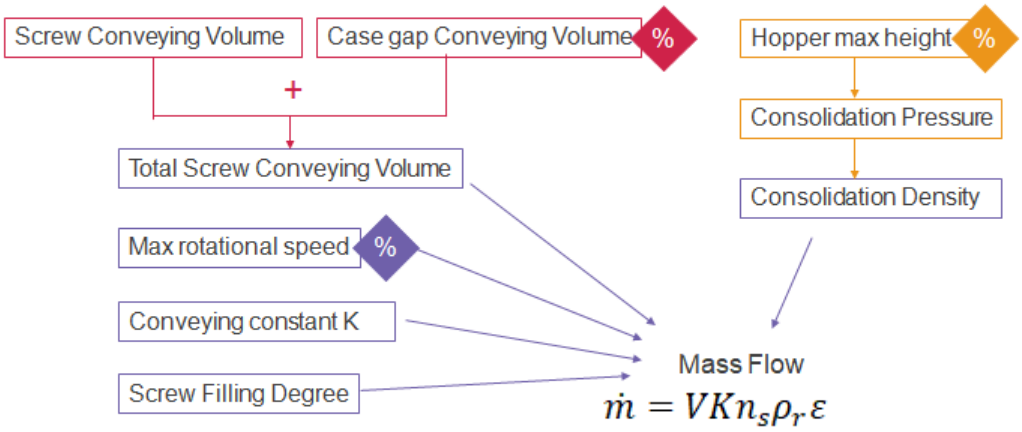

Figure 19: Mass flow calculation work flow.

The model was arranged so values of some variables could be adapted to better fit the desired scenario. The total conveying volume is defined by the sum of the screw conveying volume and the volume of the gap comprised between the screw and the screw case. This gap volume can be adjusted according to the scenario, representing the powder adhesion to the case wall. Additionally, the height of the powder bed inside the hopper can also be modified in terms of percentage of the maximum height.

The model allows predicting the mass flow of all feeder, powder and screw combinations included in it. However, for combinations not included in the dataset, a value for the $K_{ind}$is not available. In this case the mass flow prediction is only obtained through the group estimation.

It is also possible to predict the mass flow of a new powder, with the addition of few powder characteristics, e.g. ffc, wall friction angle, angle of internal friction and the compressibility data. With these values the statistical model group approximation prediction will be required to select a group conveying constant in order to predict the mass flow from this workflow.

5 Results and discussion

The model was used for the mass flow prediction of different combinations of powder, screw and feeder at different values of screw speed. As a way to analyze the accuracy of the predictions, the mass flow data from the modeling dataset was compared to the predictions. Additionally, full emptying of the hopper experiments were reproduced in the model to validate the powder densification model. Furthermore, additional powders not in the modeling dataset were used to check the accuracy of the grouped predictions.

5.1 Differences in predictions and data from the modeling dataset

In the following, the predicted mass flow values obtained by the model compared to the data obtained through the experiments and used as modeling data set was analyzed. The comparison of the values for the 20%, 50% and 80% of the maximum screw speed can be found in the Appendix, section *7.4* (*Table 7.4, Table 7.5, and Table 7.6*).

Figure 20 to *Figure 22* present the comparison of the individual K_{ind} mass flow prediction and experimental data for each screw.

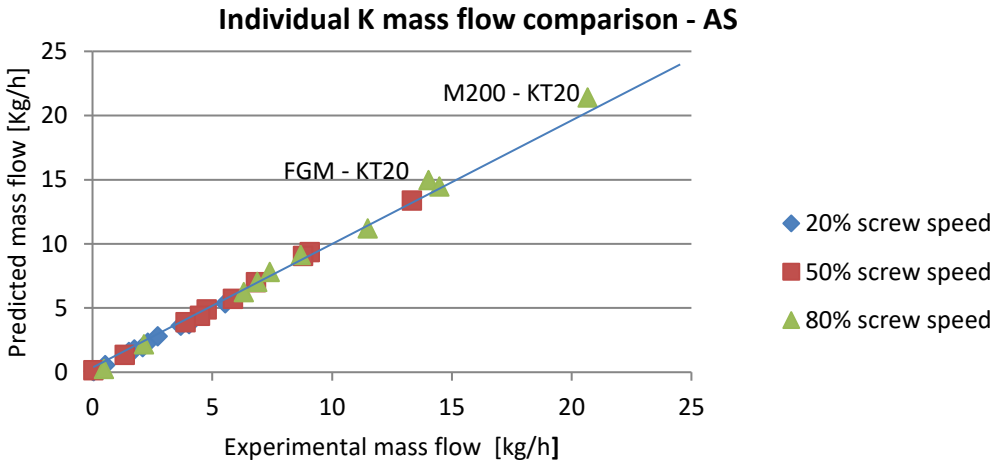

Figure 20: Comparison of experimental mass flow and individual K predictions for AS.

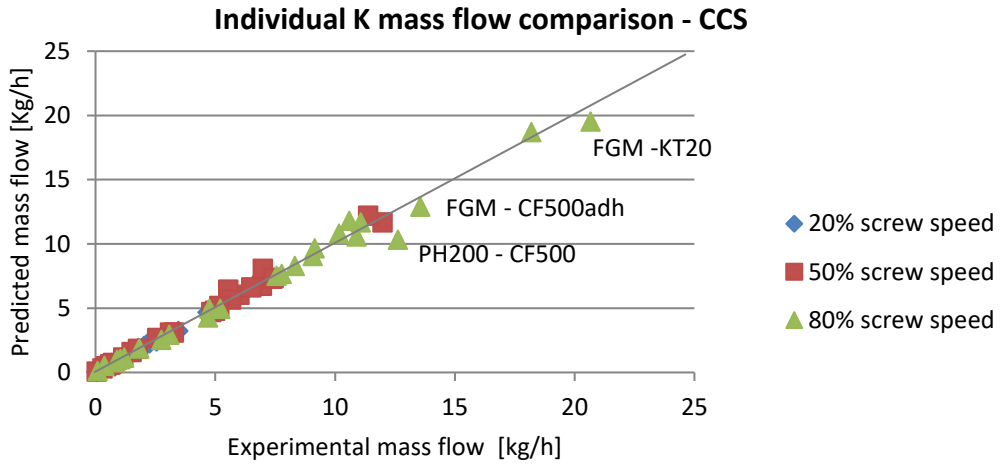

Figure 21: Comparison of experimental mass flow and individual K predictions for CCS.

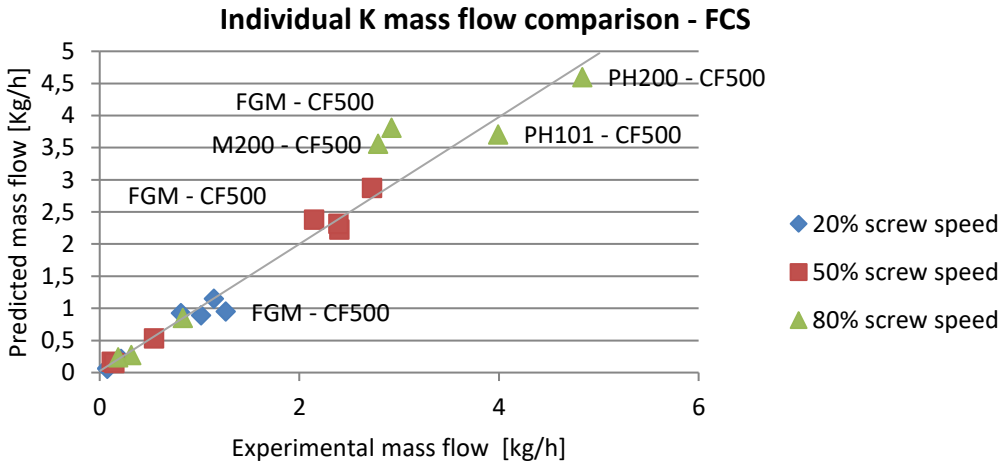

Figure 22: Comparison of experimental mass flow and individual K predictions for FCS.

The results show that the individual K_{ind} prediction is fairly precise for most of the powders. It is observed that 107 of the 126 outputs are within the 10% error margin from the experimental value. *Figure 23* shows the more detailed view of the prediction for the FGM with the CF500 feeder and CCS, representing a precise result. From the less precise values, almost half are predictions for the material PMIC, presenting values between 50% and 375% of the experimental value. A prediction obtained for PMIC is shown more detailed in *Figure 24*. The greater divergence that occurs in the PMIC predictions might come from the fact of it being a highly cohesive, compressible and electrostatically charging powder.

It can also be seen that for higher screw speeds predictions tend to get less precise than the lower screw speed predictions, with error margins going up to 50% for PMIC and 30% for the other materials. One possible reason might be that while the screw rotates faster the filling level of the screw gets compromised, contradicting the assumption of the model that the screw level has a unitary value.

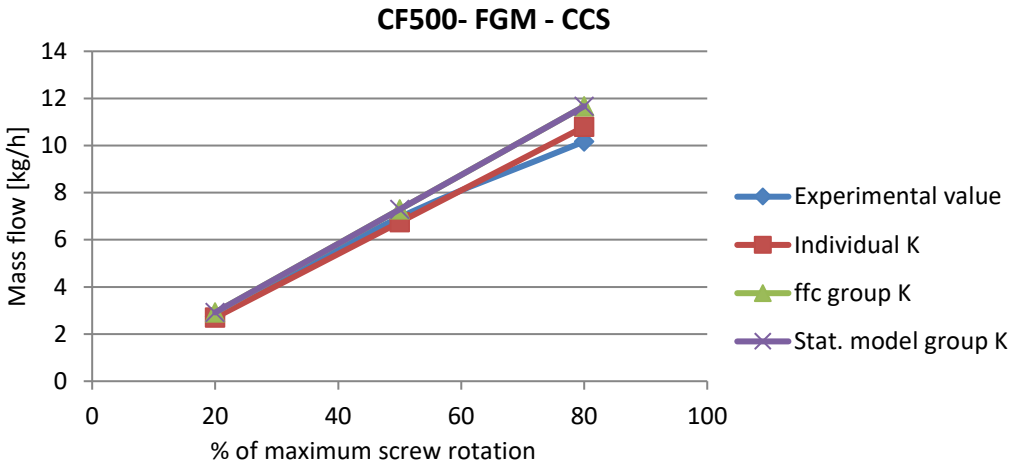

Figure 23: Mass flow comparison for FGM with the CF500 and CCS.

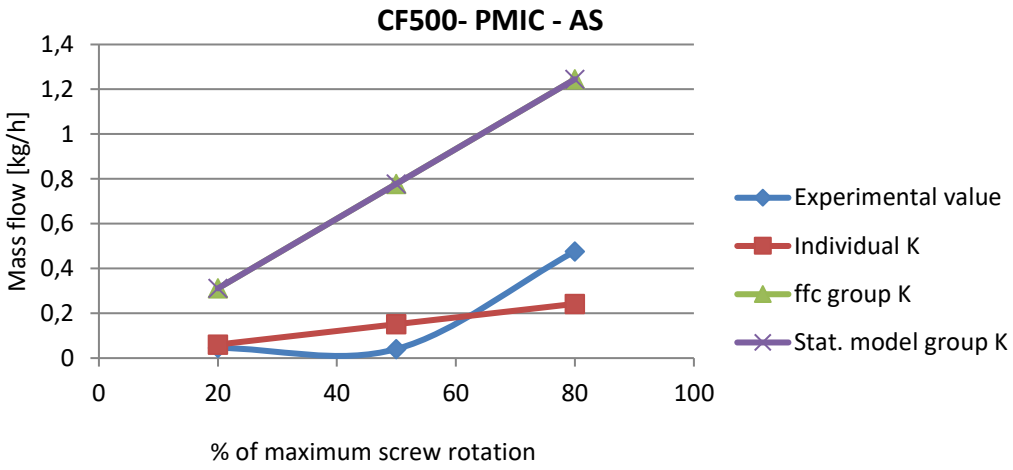

Figure 24: Mass flow comparison for PMIC with the CF500 and FCS.

5.1.1 Hopper densification model validation

To validate the powder consolidation modeling, experimental hopper emptying runs realized at 80% of the maximum screw speed were used. While the hopper is emptying the

height of the powder bed decreases, the density follows and that should reflect on the mass flow value. Only the K_{ind} mass flow was used for this analysis, since it provides the most accurate values. Therefore the variations of the density model can be easier observed.

Two of the powders, the M200 and the FGM, were considered for the analysis due to their difference in compressibility. *Figure 25* and *Figure 26* show the comparison of the two powders with the KT20 feeder and CCS.

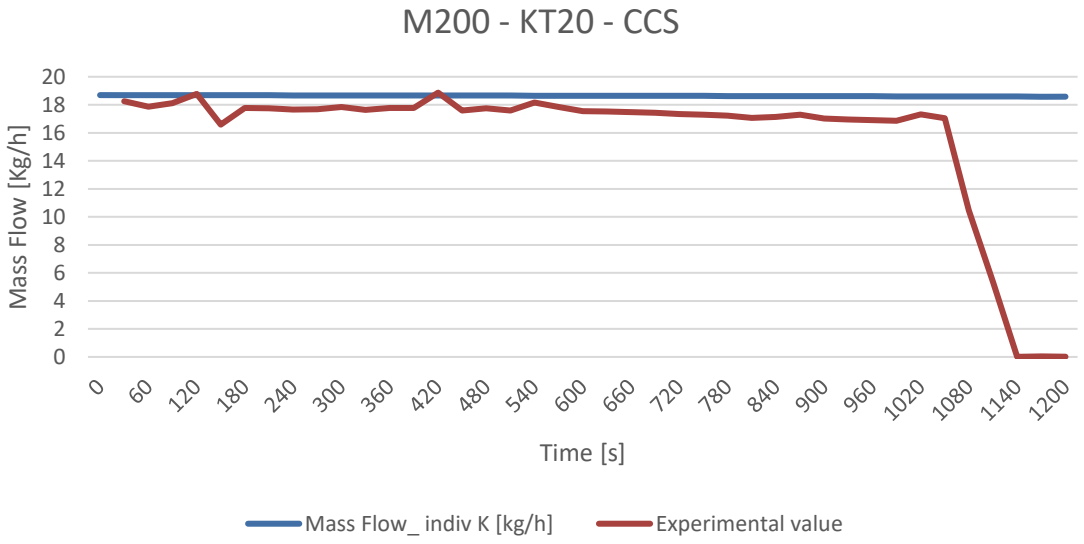

Figure 25: Hopper emptying comparison for M200 with the KT20 and CCS.

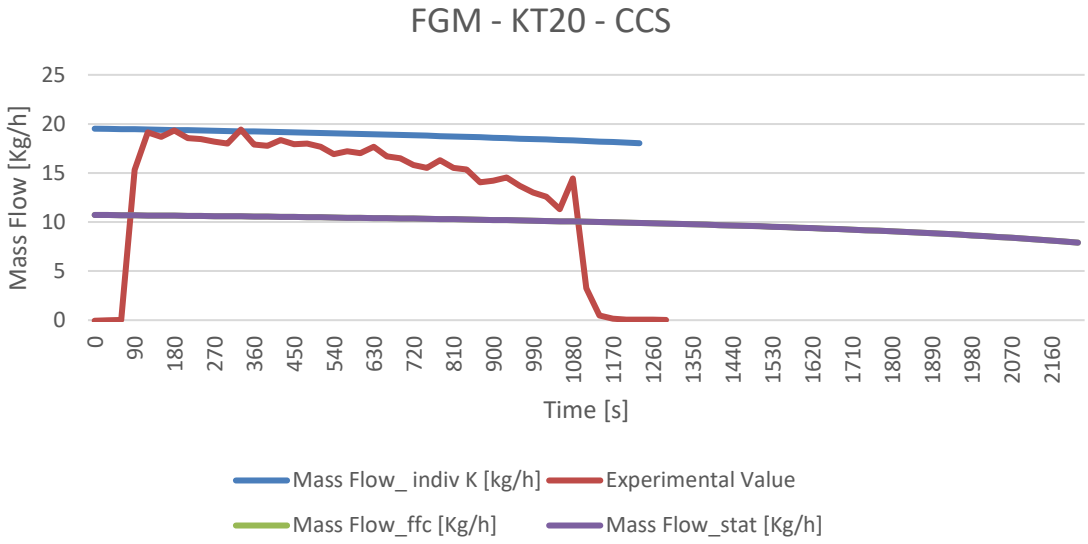

Figure 26: Hopper emptying comparison for FGM with the KT20 and CCS.

It can be observed that the M200 consolidation model is quite precise throughout the feeder emptying and the calculated mass flow has only a small variation to the experimental value. For more compressible powders like FGM, the variation of the consolidation

pressure has a bigger influence on its mass flow. The model follows the tendency, however slower than the experiment.

It can be also observed that the model cannot predict the behavior that occurs in the end of the feeding process. The big difference in mass flow at low fill levels might happen for two reasons. One reason might be the fact that the density model is fit to data from the compressibility test from 0.5 kPa to 15 kPa, while the maximum stress that acts inside of the feeder is estimated at a value around 0.5 kPa. For a more accurate density prediction a method for very loose bulk density would be needed. Another reason might be that the model does not take into consideration the effect of the agitator. When the hopper is at low levels the agitator pushes away the powder from the screw interface, interfering in the mass flow.

Additionaly, comparison for the CF500 and other screw combinations was conducted. Although the two feeder models have different hopper bottom geometries, the observations mentioned above are still valid for the CF500. The graphs for this comparison can be found in the Appendix, section *7.4.2*.

5.2 Screw conveying model validation

The mass flow predictions of the powder-feeder-screw combinations that were not included in the mass flow experimental data of the modeling dataset were calculated for the purpose of validating the group predictions. The reason for those combinations not being included in the modeling dataset being that the mass flow experiments for those were performed in different environment conditions using different batches of the raw materials which might have influenced the results of the modelling process. *Figure 27, Figure 28* and *Figure 29* show some of these results in graphical form. The summary of all results can be found in the Appendix, section 7.4.3 *(Table 7.7, Table 7.8* and *Table 7.9).*

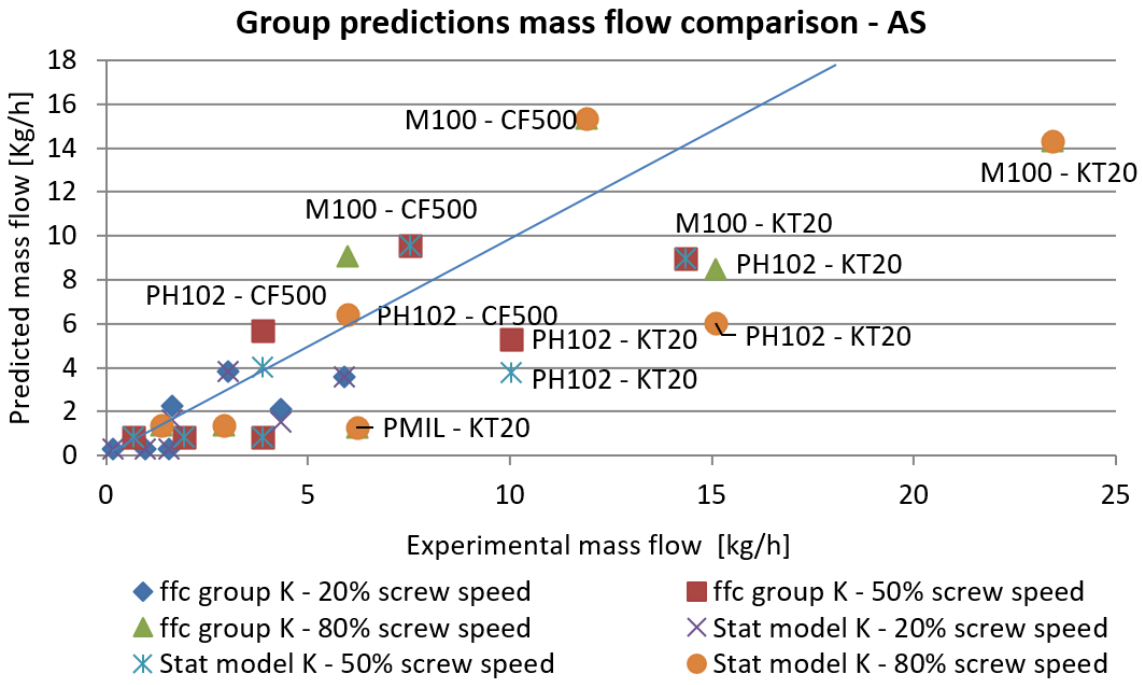

Figure 27: The comparison of group predictions and experiments mass flow for AS.

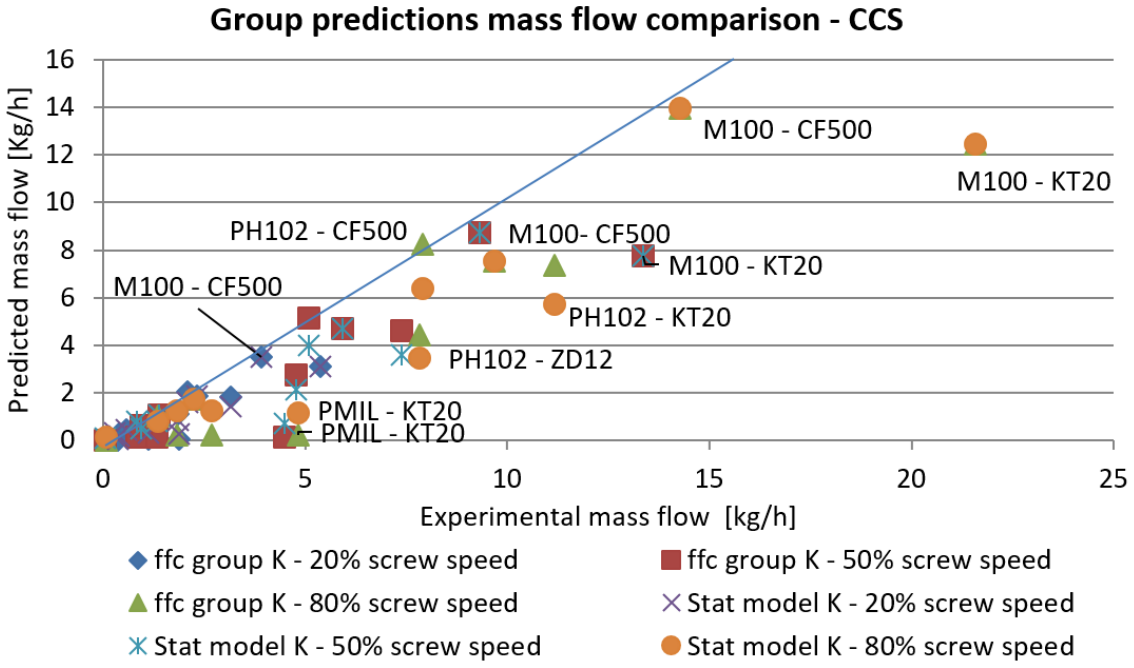

Figure 28: The comparison of group predictions and experiments mass flow for CCS.

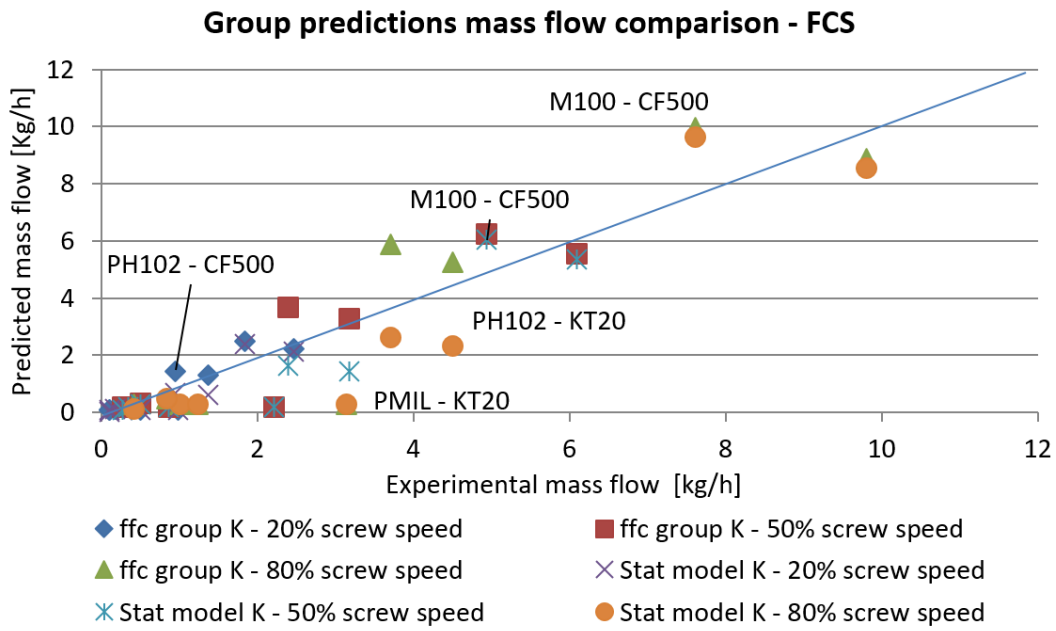

Figure 29: The comparison of group predictions and experiments mass flow for FCS

The ffc and the statistical model group K predictions are less precise than the individual prediction values. Half of the results for the ffc group and 60% of the results for the statistic model group show a deviation higher than 40% from the experimental mass flow. However, this outcome was expected, since it is a group approximation. The results could be improved if additionally to the groups of powder characteristics, groups to divide the screws by some additional classification besides their pitch length were created. This works classification does not take into consideration other dimensions that also influence the mass flow, like the pitch depth.

Observing the results, it is possible to say that the predictions involving the Compact Feeder (CF500) are the most precise comparing to other feeder's predictions. *Figure 30* shows in detail an example of a precise prediction for the CF500. The higher accuracy is probably due to the fact that the experimental data used to define the individual K_{ind} has a higher number of entries for the CF500 feeder (regular hopper and adapted hopper). As the ffc or the statistical group value K is an average of the individual K_{ind}, the value obtained is a better approximation than the value for other feeders with less entries. As a result, the prediction of material conveyed from the KT20 (with similar free screw volume) shows high deviations from the actually observed values. Among the KT20 outputs, 60% of the ffc group and 70% of the statistical model group predictions have an error margin

higher than 40%. And within these, values as high as 34% of the experimental mass flow for PH102.

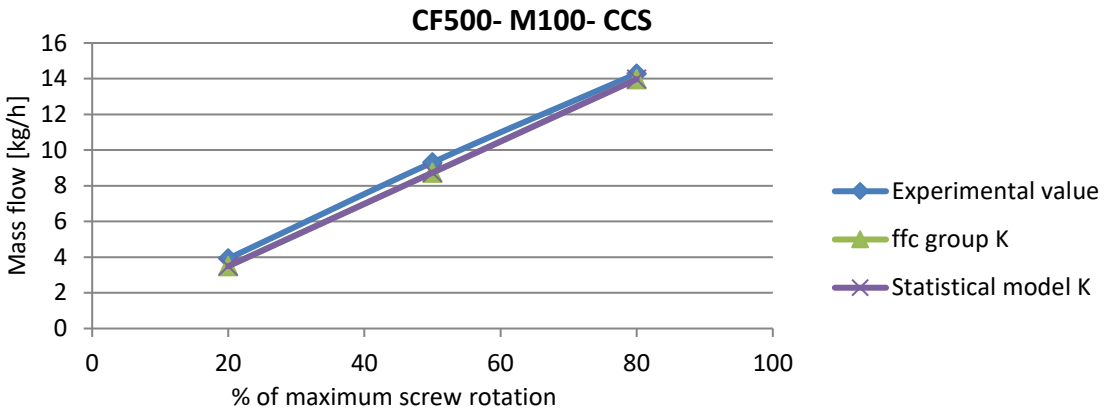

Figure 30: Mass flow comparison for the CF500 with CCS for the (a) M100, (b) PH102.

It is also observed that when predicting the mass flow for the material PMIL (*Figure 31*), all the results are not satisfactory. The reason might be the same as explained for the PMIC above. As a high compressible and electrostatically charging powder, a mass flow prediction from a simplified model (based on continuum behavior) is not possible.

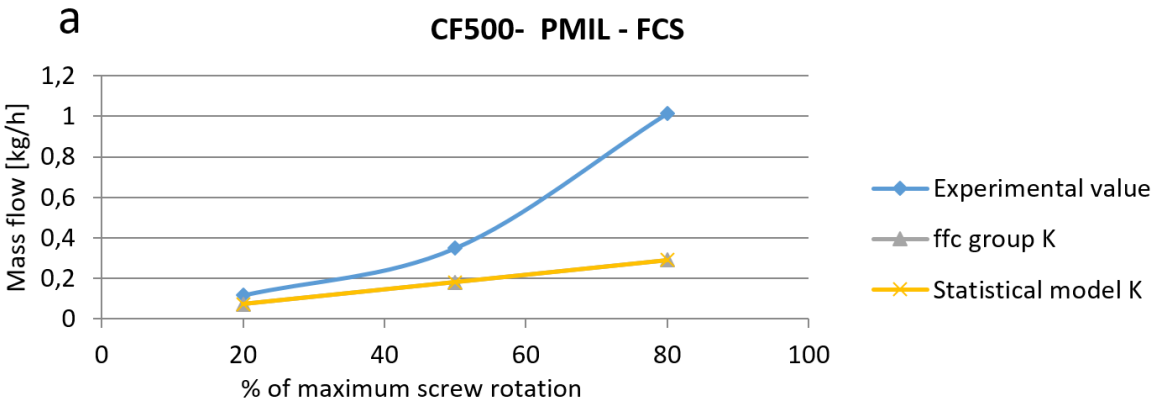

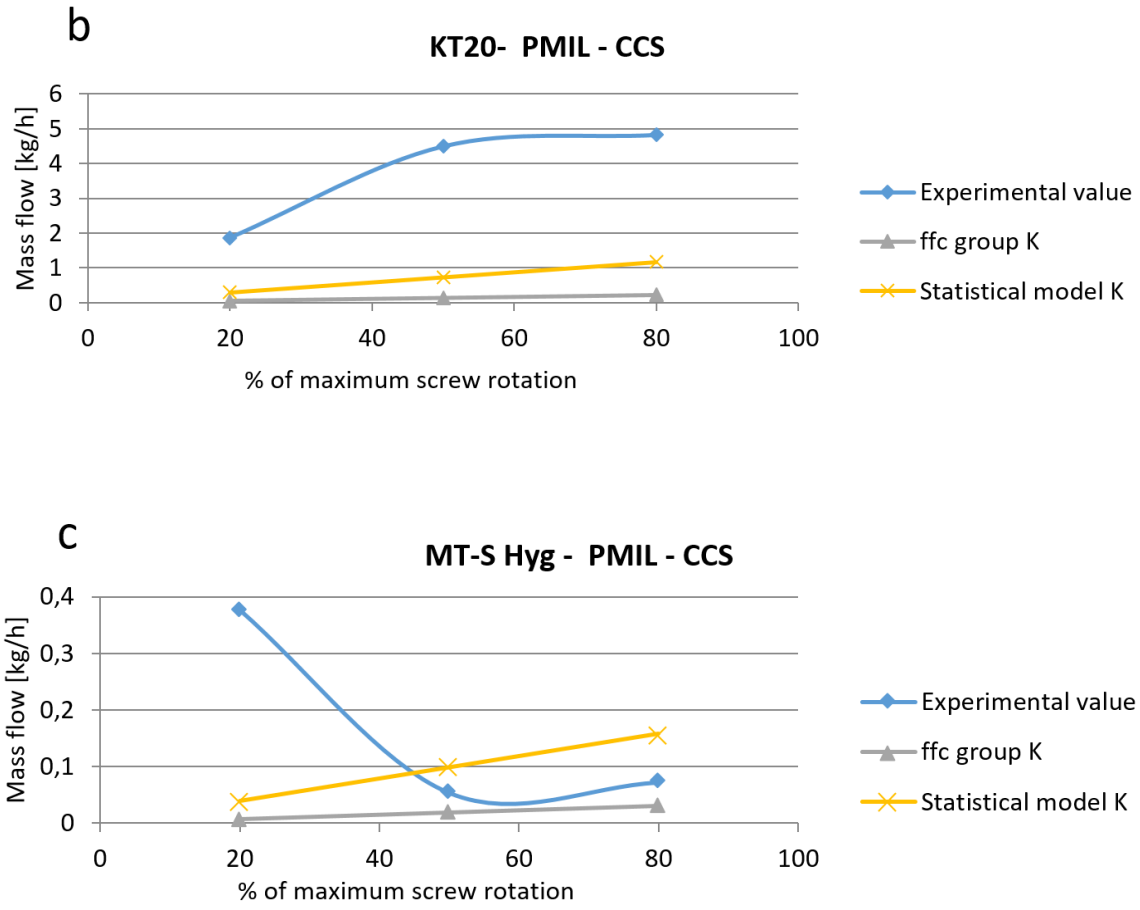

Figure 31: Mass flow comparison for the PMIL with the (a) CF500 and FCS, (b) KT20 and CCS, (c) MT-S Hyg and CCS.

5.3 Future model refinement and model limits

It has been shown that the consolidation density model gives an accurate prediction for the less compressible powders. However, for the more compressible powders the model prediction does not follow the experimental results that accurately. Also, the density behavior at the end of the feeding process cannot be represented by the given model. For a better density prediction a very loose bulk density model is needed which would fit better in the real range of stresses. The density model could also be improved with the study of the effects of the agitators in the powder.

In addition, the consolidation pressure calculation model could be improved to take into consideration the effect that the geometry of the feeder bottom causes in the powder (currently assumed to be cylindrical). The measure could result in better predictions for the feeders with rounded hopper bottoms, as the KT20 and MT-S Hyg.

The mass flow model provides a reasonable prediction for the group data. The model has been proven to be unsuitable to calculate the mass flow prediction for highly cohesive, compressible and electrostatically charging powders like the PMIC and the PMIL. Seeking an improvement of the model, a larger dataset and more balanced can be added to increase the accuracy of the predictions. Furthermore, additional DEM simulations could be made to improve the process of defining the conveying constant minimizing the experimental efforts. The powder movement inside of the twin-screw conveying space could be analyzed and new divisions of the already existing screw classification (e.g., concave screws with different pitches depths) could be created.

6 Conclusion

The work aimed to investigate mechanistic models and to develop a low order model for mass flow prediction during early process development. The model helps to increase the knowledge about the feeding process as well as to find out which impact the different powders are having on it.

Initially, a review of existing modeling approaches was performed and a model structure chosen that allows to use material characterization data in combination with geometrical descriptors of the feeders to obtain a predictive model (i.e., without feeding-experimental parameterization for each new material). Moreover, the aim was to develop a model that does not require much calculation time or large computational power. The model was then developed using as database the experimental feeding data of six powders in four different feeders equipped with diverse options of twin-screws. Three more powders were added to the study for validation of the model. The models rely on simplifications, yet they give a mechanistic estimation of the powder state in the feeding process.

Values obtained through the model with the use of the individual K_{ind} are good mass flow predictions for the most of the powders used in the study, with 85% of the results within 10% of error range. However, in the individual and group predictions it was observed that for more compressible and electrostatically charging powders like PMIC and PMIL the mass flow cannot be predicted. The group predictions have demonstrated reasonable results, except for most compressible powders. Removing the PMIC and PMIL from the analysis, the predictions done using the grouped K had 66% of their entries within 40% error margin. It was also observed that for the feeders with a flat bottomed hopper geometry, like CF500 and ZD-12 FB, the model has a better mass flow prediction. This might be due to the consolidation pressure approximation that does not take in consideration the impact that the rounded hopper bottom might have to the consolidation stress. Another reason for CF500 feeder to have a higher precision comparing to the other feeder models might be the fact that the dataset fed to the model contained more entries for it than for other feeders, resulting in a better definition of the conveying constants.

7 Appendix

7.1 Mass flow experimental value

Table 7.1: Mass Flow experimental data.

Feeder	Material	Screw	MF20 [Kg/h]	MF50[Kg/h]	MF80[Kg/h]
CF0500_GB2	FGM	FCS'	1.2604	2.1476	2.9215
CF0500_GB2	FGM	CCS'	2.7532	6.9508	10.1722
CF0500_GB2	FGM	AS'	2.3035	5.8615	8.7036
CF0500_GB2	M200	FCS'	1.0134	2.4001	2.7867
CF0500_GB2	M200	CCS'	2.5451	6.0119	9.1506
CF0500_GB2	M200	AS'	2.0974	4.7694	7.3951
CF0500_GB2	PH101	FCS'	0,8121	2,3895	3,9918
CF0500_GB2	PH101	CCS'	1.7778	4.8293	7.5634
CF0500_GB2	PH101	AS'	1.5158	3.8818	6.3211
CF0500_GB2	PH200	FCS'	1.1444	2.7278	4.8342
CF0500_GB2	PH200	CCS'	2.3546	5.5444	12.6216
CF0500_GB2	PH200	AS'	1.7473	4.4916	6.8803
CF0500_GB2	PMIC	FCS'	0.0761	0.1199	0.3164
CF0500_GB2	PMIC	CCS'	0.2000	0.4575	0.8466
CF0500_GB2	PMIC	AS'	0.0457	0.0406	0.4766
CF0500_GB2_adhopper	FGM	CCS'	3.4638	6.9803	13.5564
CF0500_GB2_adhopper	M200	CCS'	3.0355	7.3886	11.0773
CF0500_GB2_adhopper	PH101	CCS'	2.0289	5.1663	8.3198
CF0500_GB2_adhopper	PH200	CCS'	2.2529	5.6625	9.0779
CF0500_GB2_adhopper	PMIC	CCS'	0.2616	0.6159	0.9073
K-CL-KT20	FGM	CCS'	4.8565	11.3766	20.6711
K-CL-KT20	FGM	AS'	4.0313	9.0769	14.0261
K-CL-KT20	M200	CCS'	4.6759	11.9781	18.1920
K-CL-KT20	M200	AS'	5.5478	13.3340	20.6752
K-CL-KT20	PH101	CCS'	3.1375	7.4448	10.5971
K-CL-KT20	PH101	AS'	2.7225	6.8236	11.4914
K-CL-KT20	PH200	CCS'	2.5895	6.5065	10.9013
K-CL-KT20	PH200	AS'	3.6858	8.7896	14.4809
K-CL-KT20	PMIC	CCS'	0.5930	1.5084	2.7457
K-CL-KT20	PMIC	AS'	0.5359	1.3538	2.1483
MT-S Hyg	FGM	FCS'	0.0748	0.1469	0.1840
MT-S Hyg	FGM	CCS'	0.1756	0.2980	0.3752
MT-S Hyg	M200	FCS'	0.2119	0.5441	0.8323
MT-S Hyg	M200	CCS'	0.4636	1.1569	1.8338
MT-S Hyg	PH101	CCS'	0.2499	0.6356	1.0374
MT-S Hyg	PH200	CCS'	0.2820	0.7274	1.2002
ZD-12 FB	FGM	CCS'	1.2044	3.2732	4.7570
ZD-12 FB	M200	CCS'	1.8089	4.9971	7.7758
ZD-12 FB	MgSt	CCS'	0.6842	1.7799	3.0795

Feeder	Material	Screw	MF20 [Kg/h]	MF50[Kg/h]	MF80[Kg/h]
ZD-12 FB	PH101	CCS'	0.9835	2.5816	4.6960
ZD-12 FB	PH200	CCS'	1.1614	3.1168	5.2101
ZD-12 FB	PMIC	CCS'	0.0445	0.0554	0.0957

7.2 Alfa definition and curves fittings

a

	Alfa	Tension	Experimental	Prediction	SE
'Parteck M100'	0.23789423	0	0.607466667	0.61795379	0.00010998
		0.5	0.620333333	0.62097871	4.16512E-07
r_min	0.61795379	1	0.623666667	0.62344402	4.95699E-08
r_max	0.64763083	2	0.628333333	0.62722001	1.23948E-06
		4	0.632333333	0.6320766	6.59141E-08
		6	0.634333333	0.63506624	5.37146E-07
		8	0.636333333	0.6370919	5.7542E-07
		10	0.638	0.63855509	3.08122E-07
		12	0.639666667	0.63966152	2.64938E-11
		15	0.642	0.64089354	1.22425E-06
				Sum	4.41644E-06

b

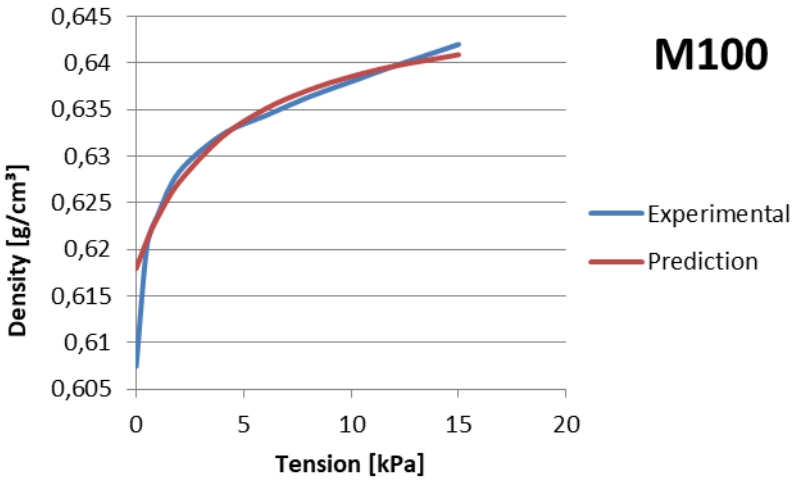

Figure 32: Alfa definition (a) and density curve fitting (b) for M100

a

	Alfa	Tension	Experimental	Prediction	SE
'Parteck M200'	0.11216375	0		0.54677607	
		0.5	0.547666667	0.54823628	3.24455E-07
		1	0.549666667	0.54955589	1.22712E-08
r_min	0.54677607	2	0.552666667	0.55184744	6.71139E-07
r_max	0.57564814	4	0.555666667	0.55540341	6.9303E-08
		6	0.557666667	0.55803494	1.35623E-07
		8	0.559666667	0.56006104	1.55527E-07
		10	0.561333333	0.56166909	1.12732E-07
		12	0.563	0.56297638	5.57974E-10
		15	0.565	0.56453526	2.15986E-07
				Sum	1.69759E-06

b

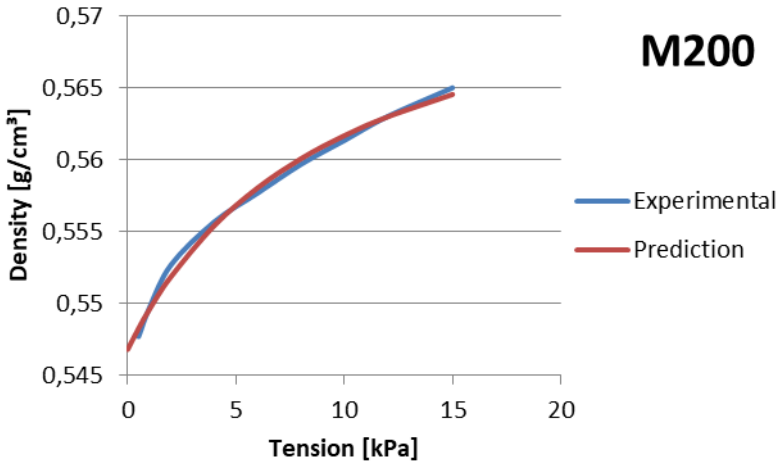

Figure 33: Alfa definition (a) and density curve fitting (b) for M200.

a

	Alfa	Tension	Experimental	Prediction	SE
'Parteck FGM'	0.25657377	0		0.53938837	
		0.5	0.560666667	0.56056489	1.03593E-08
		1	0.577666667	0.57864396	9.55109E-07
r_min	0.53938837	2	0.608333333	0.60788127	2.04359E-07
r_max	0.80777068	4	0.650666667	0.64852245	4.59767E-06
		6	0.676	0.67542978	3.25152E-07
		8	0.693	0.69455862	2.4293E-06
		10	0.706666667	0.70885597	4.79304E-06
		12	0.718	0.71994706	3.79103E-06
		15	0.736	0.73259156	1.16175E-05
				Sum	2.87235E-05

b

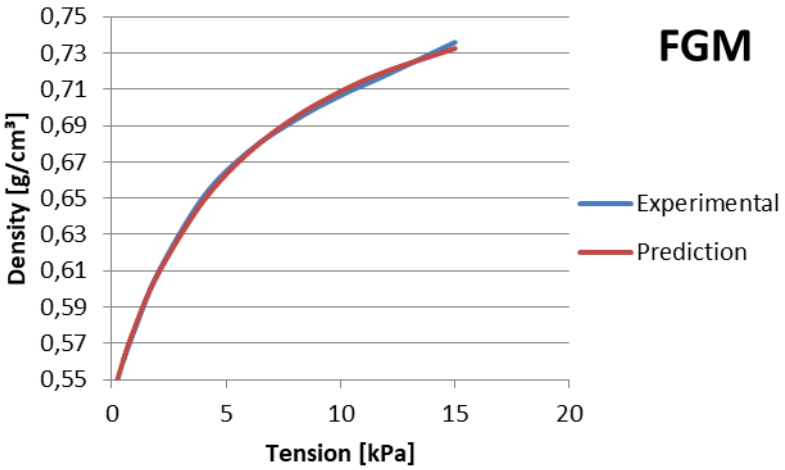

Figure 34: Alfa definition (a) and density curve fitting (b) for FGM.

a

	Alfa	Tension	Experimental	Prediction	SE
'PH102'	0.28512072	0		0.36201466	
		0.5	0.366666667	0.36733695	4.49279E-07
		1	0.372	0.37158794	1.69792E-07
r_min	0.36201466	2	0.379	0.37795306	1.09609E-06
r_max	0.40957536	4	0.385666667	0.38589032	5.00192E-08
		6	0.39	0.3906425	4.12808E-07
		8	0.393333333	0.3938064	2.2379E-07
		10	0.395666667	0.39606426	1.58079E-07
		12	0.398	0.39775652	5.92807E-08
		15	0.400333333	0.3996258	5.00606E-07
				Sum	3.11975E-06

b

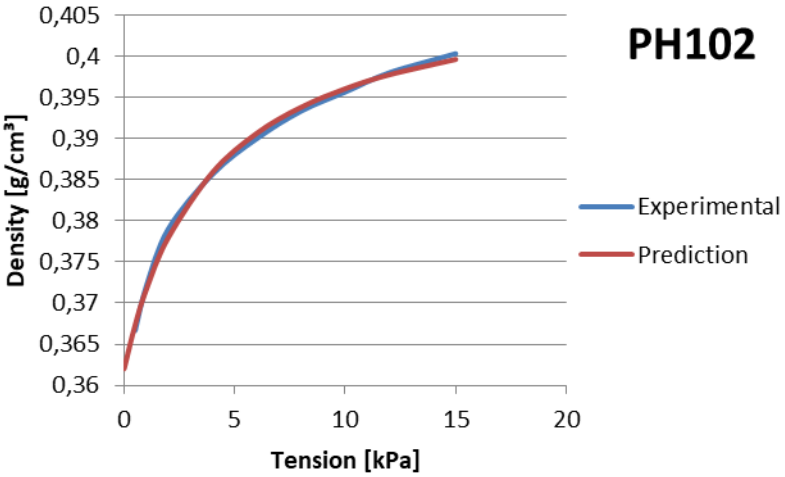

Figure 35: Alfa definition (a) and density curve fitting (b) for PH102.

a

	Alfa	Tension	Experimental	Prediction	SE
'PH200'	0.13871847	0		0.52607802	
		0.5	0.5275	0.52806219	3.16054E-07
r_min	0.52607802	1	0.53	0.52981703	3.34789E-08
r_max	0.55842846	2	0.5335	0.53278128	5.16553E-07
		4	0.5375	0.53718342	1.00221E-07
		6	0.54	0.54029576	8.74735E-08
		8	0.542	0.54261272	3.75425E-07
		10	0.544	0.54440465	1.63744E-07
		12	0.546	0.54583186	2.82722E-08
		15	0.548	0.54750012	2.49877E-07
				Sum	1.8711E-06

b

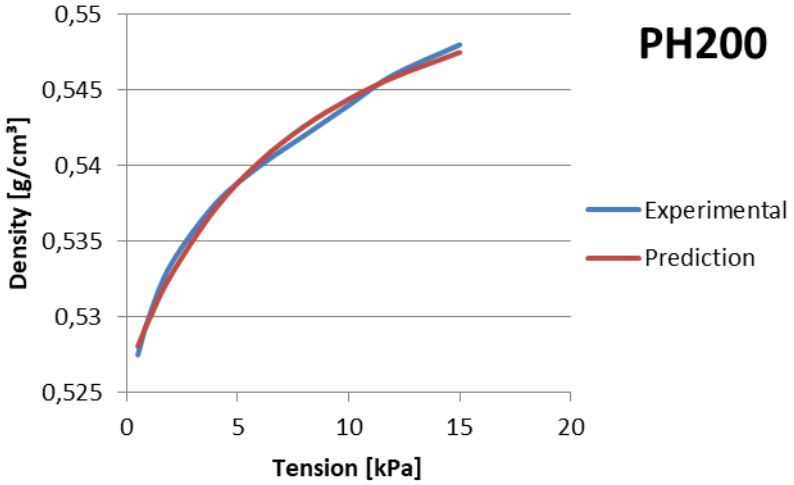

Figure 36: Alfa definition (a) and density curve fitting (b) for PH200.

a

	Alfa	Tension	Experimental	Prediction	SE
'PH101'	0.26051017	0		0.50697996	
		0.5	0.514666667	0.51555218	7.84129E-07
		1	0.523	0.52256179	1.92032E-07
r_min	0.50697996	2	0.534666667	0.53333873	1.76341E-06
r_max	0.59245924	4	0.547333333	0.54727267	3.6806E-09
		6	0.555333333	0.55589126	3.11285E-07
		8	0.561	0.56174878	5.60669E-07
		10	0.565	0.56598885	9.7782E-07
		12	0.569	0.56920014	4.00552E-08
		15	0.574333333	0.57278106	2.40954E-06
				Sum	7.04262E-06

b

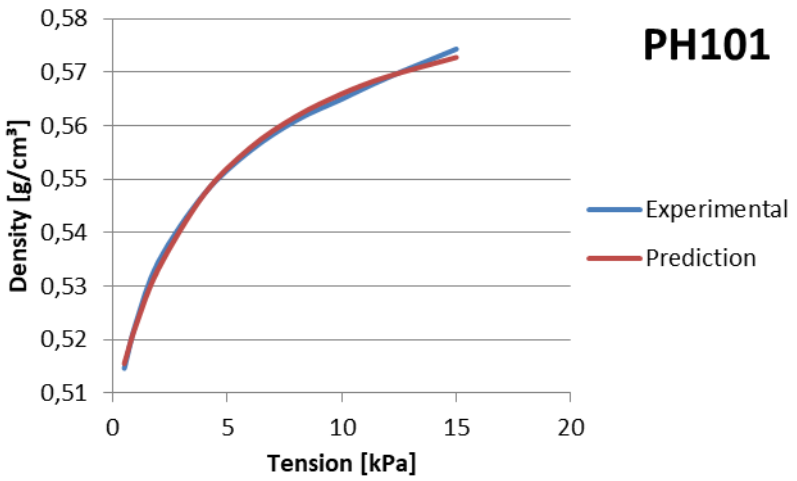

Figure 37: Alfa definition (a) and density curve fitting (b) for PH101.

a

	Alfa	Tension	Experimental	Prediction	SE
MgSt'	0.47166237	0		0.31300729	
		0.5	0.334666667	0.33800229	1.11264E-05
		1	0.360333333	0.35739502	8.63368E-06
r_min	0.31300729	2	0.389333333	0.38552823	1.44788E-05
r_max	0.51104697	4	0.418333333	0.41917221	7.03721E-07
		6	0.435333333	0.4385928	1.06241E-05
		8	0.448666667	0.45123575	6.60021E-06
		10	0.459333333	0.46012196	6.21934E-07
		12	0.467333333	0.46670926	3.89473E-07
		15	0.477333333	0.47391412	1.1691E-05
				Sum	6.48694E-05

b

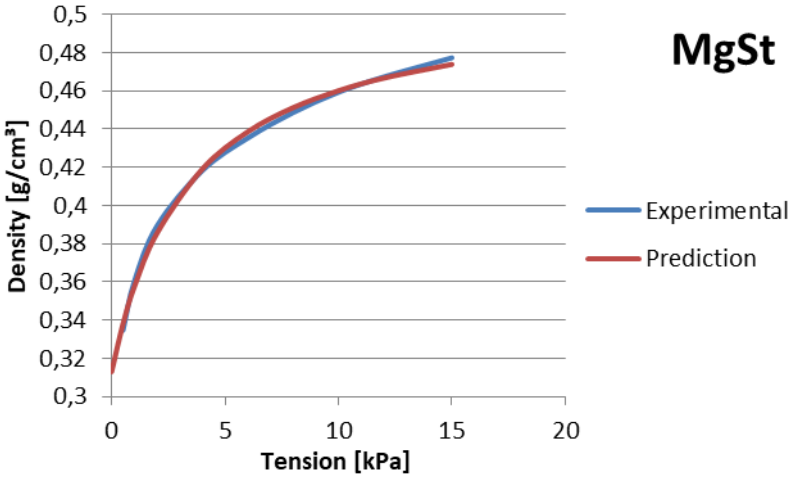

Figure 38: Alfa definition (a) and density curve fitting (b) for MgSt.

a

	Alfa	Tension	Experimental	Prediction	SE
'PMIC'	0.3336232	0		0.23144363	
		0.5	0.244666667	0.24732493	7.06636E-06
		1	0.262666667	0.26074073	3.70925E-06
r_min	0.23144363	2	0.284666667	0.28216374	6.26462E-06
r_max	0.42015815	4	0.312	0.31139549	3.65436E-07
		6	0.328666667	0.3304076	3.03084E-06
		8	0.342	0.34376194	3.10442E-06
		10	0.352333333	0.35365692	1.75187E-06
		12	0.361	0.36128259	7.98568E-08
		15	0.372666667	0.36992322	7.52649E-06
				Sum	3.28992E-05

b

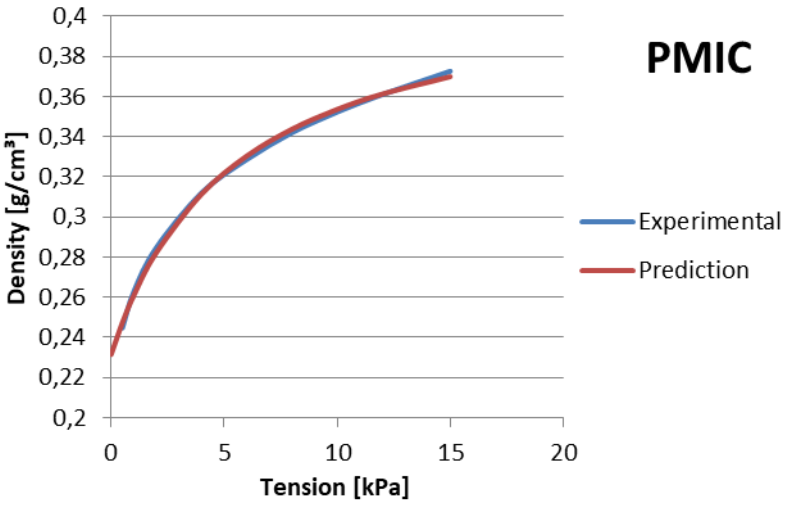

Figure 39: Alfa definition (a) and density curve fitting (b) for PMIC.

a

	Alfa	Tension	Experimental	Prediction	SE
'PMIL'	0.40500505	0		0.2438565	
		0.5	0.262666667	0.26635609	1.36118E-05
		1	0.287333333	0.28507688	5.09158E-06
r_min	0.2438565	2	0.319	0.3144424	2.07717E-05
r_max	0.48928993	4	0.354	0.35349625	2.53763E-07
		6	0.375333333	0.37828929	8.73769E-06
		8	0.392333333	0.39542672	9.56904E-06
		10	0.406333333	0.40798016	2.71205E-06
		12	0.417666667	0.41757187	8.98602E-09
		15	0.432333333	0.42835428	1.58328E-05
				Sum	7.65894E-05

b

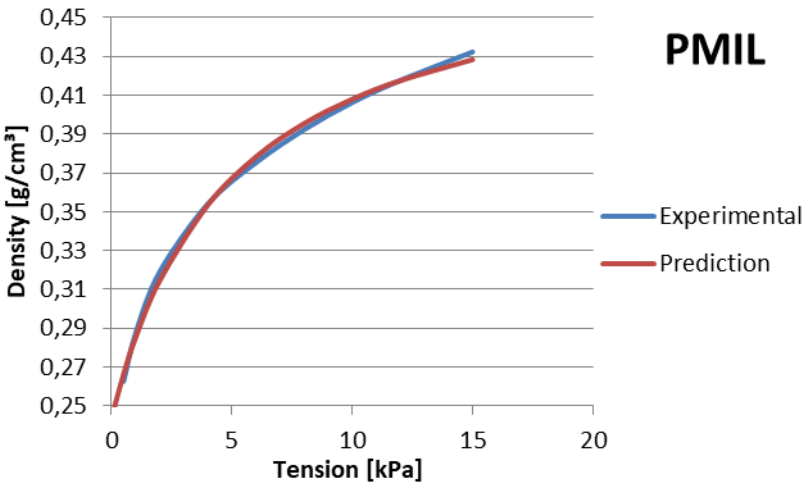

Figure 40: Alfa definition (a) and density curve fitting (b) for PMIL.

7.3 Influences in the conveying constant value

Table 7.2: Gap volume influence in the K_ind value

Feeder	Material	Screw	K_ind average V with gap	K_ind average V without gap	% difference
CF0500_GB2	FGM	'AS'	0.0188	0.0239	1.2714
CF0500_GB2	M200	'AS'	0.0165	0.0210	1.2714
CF0500_GB2	PH101	'AS'	0.0140	0.0178	1.2714
CF0500_GB2	PMIC	'AS'	0.0012	0.0015	1.2714
CF0500_GB2	PH200	'AS'	0.0154	0.0196	1.2714
CF0500_GB2	PH101	'FCS'	0.0269	0.0330	1.2243
CF0500_GB2	PMIC	'FCS'	0.0112	0.0137	1.2243
CF0500_GB2	FGM	'FCS'	0.0331	0.0405	1.2243
CF0500_GB2	M200	'FCS'	0.0486	0.0596	1.2243
CF0500_GB2	PH200	'FCS'	0.0341	0.0417	1.2243
CF0500_GB2_adhopper	FGM	'AS'	0.0130	0.0146	1.1315
CF0500_GB2_adhopper	M200	'AS'	0.0118	0.0134	1.1315
CF0500_GB2_adhopper	PH101	'AS'	0.0098	0.0111	1.1315
CF0500_GB2_adhopper	PMIC	'AS'	0.0022	0.0025	1.1315
CF0500_GB2_adhopper	PH200	'AS'	0.0131	0.0149	1.1315
CF0500_GB2_adhopper	PH101	'CCS'	0.0108	0.0122	1.1315
CF0500_GB2_adhopper	FGM	'CCS'	0.0154	0.0174	1.1315
CF0500_GB2_adhopper	M200	'CCS'	0.0143	0.0162	1.1315
CF0500_GB2_adhopper	PMIC	'CCS'	0.0028	0.0031	1.1315
CF0500_GB2_adhopper	PH200	'CCS'	0.0115	0.0131	1.1315
CF0500_GB2_adhopper	PH101	'FCS'	0.0173	0.0232	1.3438
CF0500_GB2_adhopper	PMIC	'FCS'	0.0080	0.0107	1.3438
CF0500_GB2_adhopper	FGM	'FCS'	0.0263	0.0353	1.3438

Feeder	Material	Screw	K_ind average V with gap	K_ind average V without gap	% difference
CF0500_GB2_adhopper	M200	'FCS'	0.0259	0.0348	1.3438
CF0500_GB2_adhopper	PH200	'FCS'	0.0152	0.0204	1.3438
K-CL-KT20	PH101	'AS'	0.0106	0.0131	1.2313
K-CL-KT20	FGM	'AS'	0.0048	0.0060	1.2313
K-CL-KT20	M200	'AS'	0.0182	0.0225	1.2313
K-CL-KT20	PH200	'AS'	0.0119	0.0147	1.2313
K-CL-KT20	PH101	'CCS'	0.0102	0.0128	1.2501
K-CL-KT20	PMIC	'CCS'	0.0006	0.0008	1.2501
K-CL-KT20	FGM	'CCS'	0.0106	0.0133	1.2501
K-CL-KT20	M200	'CCS'	0.0174	0.0218	1.2501
K-CL-KT20	PH200	'CCS'	0.0117	0.0146	1.2501
K-CL-KT20	MgSt	'CCS'	0.0107	0.0133	1.2501
MT-S Hyg	FGM	'CCS'	0.0045	0.0052	1.1414
MT-S Hyg	M200	'CCS'	0.0044	0.0050	1.1414
MT-S Hyg	PMIC	'CCS'	0.0008	0.0009	1.1414
MT-S Hyg	PH200	'CCS'	0.0058	0.0067	1.1414
ZD-12 FB	FGM	'CCS'	0.0061	0.0075	1.2313
ZD-12 FB	M200	'CCS'	0.0222	0.0273	1.2313

Table 7.3: Bulk density influence in the K_ind value

Feeder	Material	Screw	K_ind min density	K_average Min density=BD	% diference
CF0500_GB2	FGM	'AS'	0.0188	0.0200	1.0644
CF0500_GB2	M200	'AS'	0.0165	0.0175	1.0600
CF0500_GB2	PH101	'AS'	0.0140	0.0206	1.4688
CF0500_GB2	PMIC	'AS'	0.0012	0.0013	1.0946
CF0500_GB2	PH200	'AS'	0.0154	0.0228	1.4794
CF0500_GB2	PH101	'FCS'	0.0270	0.0396	1.4688
CF0500_GB2	PMIC	'FCS'	0.0112	0.0123	1.0946
CF0500_GB2	FGM	'FCS'	0.0330	0.0352	1.0644
CF0500_GB2	M200	'FCS'	0.0486	0.0516	1.0600
CF0500_GB2	PH200	'FCS'	0.0341	0.0504	1.4794
CF0500_GB2_adhopper	FGM	'AS'	0.0129	0.0137	1.0644
CF0500_GB2_adhopper	M200	'AS'	0.0118	0.0125	1.0600
CF0500_GB2_adhopper	PH101	'AS'	0.0098	0.0144	1.4688
CF0500_GB2_adhopper	PMIC	'AS'	0.0022	0.0024	1.0946
CF0500_GB2_adhopper	PH200	'AS'	0.0131	0.0194	1.4794
CF0500_GB2_adhopper	PH101	'CCS'	0.0108	0.0158	1.4688
CF0500_GB2_adhopper	FGM	'CCS'	0.0154	0.0164	1.0644
CF0500_GB2_adhopper	M200	'CCS'	0.0143	0.0152	1.0600
CF0500_GB2_adhopper	PMIC	'CCS'	0.0028	0.0030	1.0946

Feeder	Material	Screw	K_ind min density	K_average Min density=BD	% diference
CF0500_GB2_adhopper	PH200	'CCS'	0.0115	0.0171	1.4794
CF0500_GB2_adhopper	PH101	'FCS'	0.0173	0.0254	1.4688
CF0500_GB2_adhopper	PMIC	'FCS'	0.0080	0.0087	1.0946
CF0500_GB2_adhopper	FGM	'FCS'	0.0263	0.0280	1.0644
CF0500_GB2_adhopper	M200	'FCS'	0.0259	0.0274	1.0600
CF0500_GB2_adhopper	PH200	'FCS'	0.0152	0.0225	1.4794
K-CL-KT20	PH101	'AS'	0.0106	0.0152	1.4323
K-CL-KT20	FGM	'AS'	0.0048	0.0051	1.0592
K-CL-KT20	M200	'AS'	0.0182	0.0192	1.0565
K-CL-KT20	PH200	'AS'	0.0119	0.0173	1.4534
K-CL-KT20	PH101	'CCS'	0.0102	0.0146	1.4323
K-CL-KT20	PMIC	'CCS'	0.0006	0.0007	1.0905
K-CL-KT20	FGM	'CCS'	0.0106	0.0112	1.0592
K-CL-KT20	M200	'CCS'	0.0174	0.0184	1.0565
K-CL-KT20	PH200	'CCS'	0.0117	0.0170	1.4534
K-CL-KT20	MgSt	'CCS'	0.0107	0.0143	1.3424
MT-S Hyg	FGM	'CCS'	0.0045	0.0048	1.0642
MT-S Hyg	M200	'CCS'	0.0044	0.0046	1.0595
MT-S Hyg	PMIC	'CCS'	0.0008	0.0008	1.0939
MT-S Hyg	PH200	'CCS'	0.0058	0.0086	1.4725
ZD-12 FB	FGM	'CCS'	0.0061	0.0065	1.0652
ZD-12 FB	M200	'CCS'	0.0222	0.0235	1.0604

7.4 Mass flow predictions

7.4.1 Experimental and prediction mass flow comparison from the modeling dataset

Table 7.4: Mass flow experimental values and predictions to 20% of screw speed

Feeder	Powder	Screw	Experimental mass flow	Individual K mass flow	ffc group mass flow	Stat model group mass flow
CF0500_GB2	M200	AS'	2.0974	1.9517	3.3832	3.3832
CF0500_GB2	M200	CCS'	2.5451	2.4130	3.0813	3.0813
CF0500_GB2	M200	FCS'	1.0134	0.8902	2.1988	2.1236
CF0500_GB2	FGM	AS'	2.3035	2.2804	3.0781	3.0781
CF0500_GB2	FGM	CCS'	2.7532	2.6990	2.9170	2.9170
CF0500_GB2	FGM	FCS'	1.2604	0.9523	1.1123	1.1123
CF0500_GB2	PH200	AS'	1.7473	1.7572	3.2594	3.2594
CF0500_GB2	PH200	CCS'	2.3547	2.5796	2.9686	2.9686
CF0500_GB2	PH200	FCS'	1.1444	1.1496	2.1184	2.0459
CF0500_GB2	PH101	AS'	1.5158	1.5584	2.2619	2.2619
CF0500_GB2	PH101	CCS'	1.7778	1.8774	2.2344	2.2543
CF0500_GB2	PH101	FCS'	0.8120	0.9271	0.9271	0.9271

Feeder	Powder	Screw	Experimental mass flow	Individual K mass flow	ffc group mass flow	Stat model group mass flow
CF0500_GB2	PMIC	AS'	0.0457	0.0606	0.3112	0.3112
CF0500_GB2	PMIC	CCS'	0.2000	0.1988	0.2972	0.2972
CF0500_GB2	PMIC	FCS'	0.0761	0.0679	0.0679	0.0679
CF0500_GB2_adh	M200	CCS'	3.0355	2.9206	3.0813	3.0813
CF0500_GB2_adh	FGM	CCS'	3.4638	3.2231	2.9170	2.9170
CF0500_GB2_adh	PH200	CCS'	2.2530	2.2657	2.9686	2.9686
CF0500_GB2_adh	PH101	CCS'	2.0289	2.0701	2.2344	2.2543
CF0500_GB2_adh	PMIC	CCS'	0.2616	0.2457	0.2972	0.2972
K-CL-KT20	M200	AS'	5.5478	5.3518	3.1556	3.1556
K-CL-KT20	M200	CCS'	4.6759	4.6732	2.7375	2.7375
K-CL-KT20	FGM	AS'	4.0313	3.7387	2.9693	2.9693
K-CL-KT20	FGM	CCS'	4.8565	4.8790	2.6803	2.6803
K-CL-KT20	PH200	AS'	3.6858	3.6169	3.0444	3.0444
K-CL-KT20	PH200	CCS'	2.5895	2.6462	2.6410	2.6410
K-CL-KT20	PH101	AS'	2.7225	2.8020	2.1373	2.1373
K-CL-KT20	PH101	CCS'	3.1375	2.9501	2.0110	2.0290
K-CL-KT20	PMIC	AS'	0.5359	0.5412	0.2998	0.2998
K-CL-KT20	PMIC	CCS'	0.5930	0.6312	0.2727	0.2727
MT-S Hyg	M200	CCS'	0.4636	0.4617	0.3825	0.3825
MT-S Hyg	M200	FCS'	0.2119	0.2126	0.1036	0.1000
MT-S Hyg	FGM	CCS'	0.1756	0.1299	0.3626	0.3626
MT-S Hyg	FGM	FCS'	0.0748	0.0600	0.0525	0.0525
MT-S Hyg	PH200	CCS'	0.2820	0.2915	0.3688	0.3688
MT-S Hyg	PH101	CCS'	0.2499	0.2561	0.2780	0.2805
ZD-12 FB	M200	CCS'	1.8089	1.9175	1.6595	1.6595
ZD-12 FB	FGM	CCS'	1.2044	1.2371	1.5633	1.5633
ZD-12 FB	PH200	CCS'	1.1614	1.2385	1.5987	1.5987
ZD-12 FB	PH101	CCS'	0.9835	1.0688	1.2014	1.2121
ZD-12 FB	MgSt	CCS'	0.6842	0.7310	0.7651	0.7310
ZD-12 FB	PMIC	CCS'	0.0445	0.0303	0.0303	0.1595

Table 7.5: Mass flow experimental values and predictions to 50% of screw speed

Feeder	Powder	Screw	Experimental mass flow	Individual K mass flow	ffc group mass flow	Stat model group mass flow
CF0500_GB2	M200	AS'	4.7695	4.8792	8.4579	8.4579
CF0500_GB2	M200	CCS'	6.0120	6.0324	7.7032	7.7032
CF0500_GB2	M200	FCS'	2.4001	2.2255	5.4970	5.3089
CF0500_GB2	FGM	AS'	5.8615	5.7010	7.6951	7.6951
CF0500_GB2	FGM	CCS'	6.9508	6.7475	7.2926	7.2926
CF0500_GB2	FGM	FCS'	2.1476	2.3808	2.7808	2.7808
CF0500_GB2	PH200	AS'	4.4916	4.3929	8.1486	8.1486

Feeder	Powder	Screw	Experimental mass flow	Individual K mass flow	ffc group mass flow	Stat model group mass flow
CF0500_GB2	PH200	CCS'	5.5444	6.4489	7.4214	7.4214
CF0500_GB2	PH200	FCS'	2.7279	2.8741	5.2960	5.1148
CF0500_GB2	PH101	AS'	3.8818	3.8960	5.6548	5.6548
CF0500_GB2	PH101	CCS'	4.8293	4.6935	5.5860	5.6358
CF0500_GB2	PH101	FCS'	2.3895	2.3178	2.3178	2.3178
CF0500_GB2	PMIC	AS'	0.0406	0.1514	0.7780	0.7780
CF0500_GB2	PMIC	CCS'	0.4575	0.4970	0.7430	0.7430
CF0500_GB2	PMIC	FCS'	0.1199	0.1698	0.1698	0.1698
CF0500_GB2_adh	M200	CCS'	7.3886	7.3015	7.7032	7.7032
CF0500_GB2_adh	FGM	CCS'	6.9803	8.0578	7.2926	7.2926
CF0500_GB2_adh	PH200	CCS'	5.6625	5.6642	7.4214	7.4214
CF0500_GB2_adh	PH101	CCS'	5.1663	5.1753	5.5860	5.6358
CF0500_GB2_adh	PMIC	CCS'	0.6159	0.6142	0.7430	0.7430
K-CL-KT20	M200	AS'	13.3340	13.3795	7.8890	7.8890
K-CL-KT20	M200	CCS'	11.9781	11.6831	6.8437	6.8437
K-CL-KT20	FGM	AS'	9.0769	9.3468	7.4231	7.4231
K-CL-KT20	FGM	CCS'	11.3766	12.1974	6.7007	6.7007
K-CL-KT20	PH200	AS'	8.7896	9.0422	7.6110	7.6110
K-CL-KT20	PH200	CCS'	6.5065	6.6154	6.6026	6.6026
K-CL-KT20	PH101	AS'	6.8236	7.0051	5.3432	5.3432
K-CL-KT20	PH101	CCS'	7.4449	7.3752	5.0275	5.0724
K-CL-KT20	PMIC	AS'	1.3538	1.3531	0.7494	0.7494
K-CL-KT20	PMIC	CCS'	1.5084	1.5779	0.6817	0.6817
MT-S Hyg	M200	CCS'	1.1569	1.1542	0.9562	0.9562
MT-S Hyg	M200	FCS'	0.5441	0.5315	0.2590	0.2501
MT-S Hyg	FGM	CCS'	0.2980	0.3247	0.9066	0.9066
MT-S Hyg	FGM	FCS'	0.1469	0.1501	0.1312	0.1312
MT-S Hyg	PH200	CCS'	0.7274	0.7288	0.9220	0.9220
MT-S Hyg	PH101	CCS'	0.6356	0.6403	0.6950	0.7012
ZD-12 FB	M200	CCS'	4.9971	4.7938	4.1487	4.1487
ZD-12 FB	FGM	CCS'	3.2732	3.0928	3.9083	3.9083
ZD-12 FB	PH200	CCS'	3.1168	3.0962	3.9966	3.9966
ZD-12 FB	PH101	CCS'	2.5817	2.6720	3.0035	3.0303
ZD-12 FB	MgSt	CCS'	1.7799	1.8275	1.9128	1.8275
ZD-12 FB	PMIC	CCS'	0.0554	0.0757	0.0757	0.3987

Table 7.6: Mass flow experimental values and predictions to 80% of screw speed

Feeder	Powder	Screw	Experimental mass flow	Individual K mass flow	ffc group mass flow	Stat model group mass flow
CF0500_GB2	M200	AS'	7.3951	7.8067	13.5327	13.5327
CF0500_GB2	M200	CCS'	9.1506	9.6518	12.3251	12.3251
CF0500_GB2	M200	FCS'	2.7867	3.5608	8.7952	8.4943
CF0500_GB2	FGM	AS'	8.7036	9.1217	12.3122	12.3122
CF0500_GB2	FGM	CCS'	10.1722	10.7960	11.6682	11.6682
CF0500_GB2	FGM	FCS'	2.9215	3.8093	4.4492	4.4492
CF0500_GB2	PH200	AS'	6.8803	7.0286	13.0378	13.0378
CF0500_GB2	PH200	CCS'	12.6216	10.3183	11.8743	11.8743
CF0500_GB2	PH200	FCS'	4.8342	4.5986	8.4735	8.1836
CF0500_GB2	PH101	AS'	6.3211	6.2336	9.0477	9.0477
CF0500_GB2	PH101	CCS'	7.5634	7.5095	8.9376	9.0174
CF0500_GB2	PH101	FCS'	3.9917	3.7086	3.7086	3.7086
CF0500_GB2	PMIC	AS'	0.4766	0.2422	1.2449	1.2449
CF0500_GB2	PMIC	CCS'	0.8466	0.7953	1.1888	1.1888
CF0500_GB2	PMIC	FCS'	0.3164	0.2717	0.2717	0.2717
CF0500_GB2_adh	M200	CCS'	11.0773	11.6824	12.3251	12.3251
CF0500_GB2_adh	FGM	CCS'	13.5564	12.8926	11.6682	11.6682
CF0500_GB2_adh	PH200	CCS'	9.0779	9.0627	11.8743	11.8743
CF0500_GB2_adh	PH101	CCS'	8.3198	8.2805	8.9376	9.0174
CF0500_GB2_adh	PMIC	CCS'	0.9073	0.9827	1.1888	1.1888
K-CL-KT20	M200	AS'	20.6752	21.4072	12.6224	12.6224
K-CL-KT20	M200	CCS'	18.1920	18.6930	10.9500	10.9500
K-CL-KT20	FGM	AS'	14.0261	14.9548	11.8770	11.8770
K-CL-KT20	FGM	CCS'	20.6711	19.5159	10.7212	10.7212
K-CL-KT20	PH200	AS'	14.4809	14.4676	12.1776	12.1776
K-CL-KT20	PH200	CCS'	10.9013	10.5846	10.5641	10.5641
K-CL-KT20	PH101	AS'	11.4914	11.2082	8.5491	8.5491
K-CL-KT20	PH101	CCS'	10.5971	11.8003	8.0440	8.1158
K-CL-KT20	PMIC	AS'	2.1483	2.1649	1.1991	1.1991
K-CL-KT20	PMIC	CCS'	2.7457	2.5246	1.0907	1.0907
MT-S Hyg	M200	CCS'	1.8338	1.8468	1.5299	1.5299
MT-S Hyg	M200	FCS'	0.8323	0.8504	0.4143	0.4002
MT-S Hyg	FGM	CCS'	0.3752	0.5195	1.4505	1.4505
MT-S Hyg	FGM	FCS'	0.1841	0.2401	0.2099	0.2099
MT-S Hyg	PH200	CCS'	1.2002	1.1661	1.4751	1.4751
MT-S Hyg	PH101	CCS'	1.0374	1.0245	1.1120	1.1219
ZD-12 FB	M200	CCS'	7.7758	7.6701	6.6379	6.6379
ZD-12 FB	FGM	CCS'	4.7570	4.9484	6.2532	6.2532
ZD-12 FB	PH200	CCS'	5.2101	4.9538	6.3946	6.3946
ZD-12 FB	PH101	CCS'	4.6960	4.2752	4.8056	4.8485
ZD-12 FB	MgSt	CCS'	3.0796	2.9240	3.0606	2.9240
ZD-12 FB	PMIC	CCS'	0.0957	0.1211	0.1211	0.6379

7.4.2 Hopper emptying predicted and experimental mass flow comparison

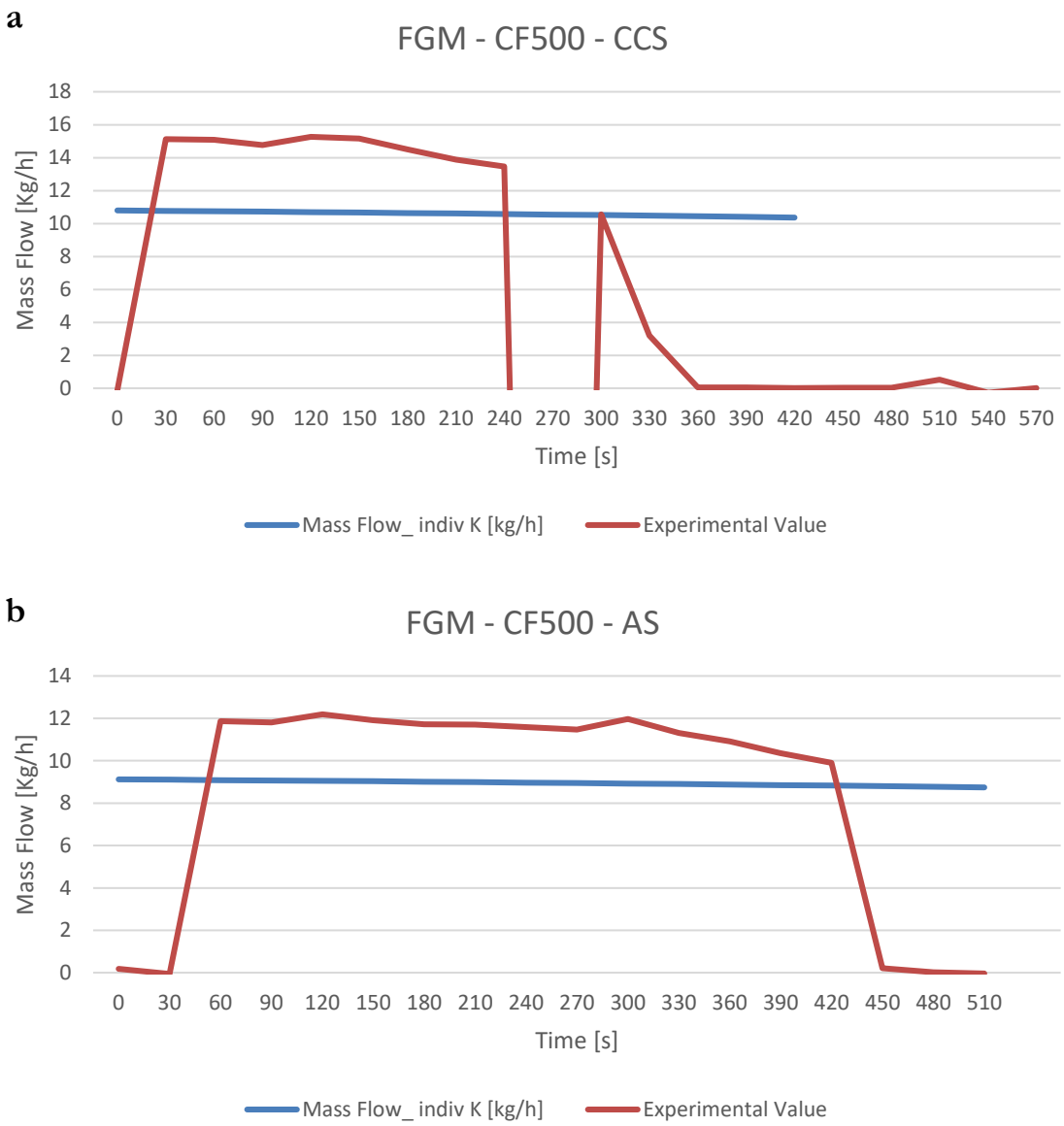

Figure 41: Mass flow experimental and predicted values comparison for the FGM together with CF500 and (a)CCS and (b)AS.

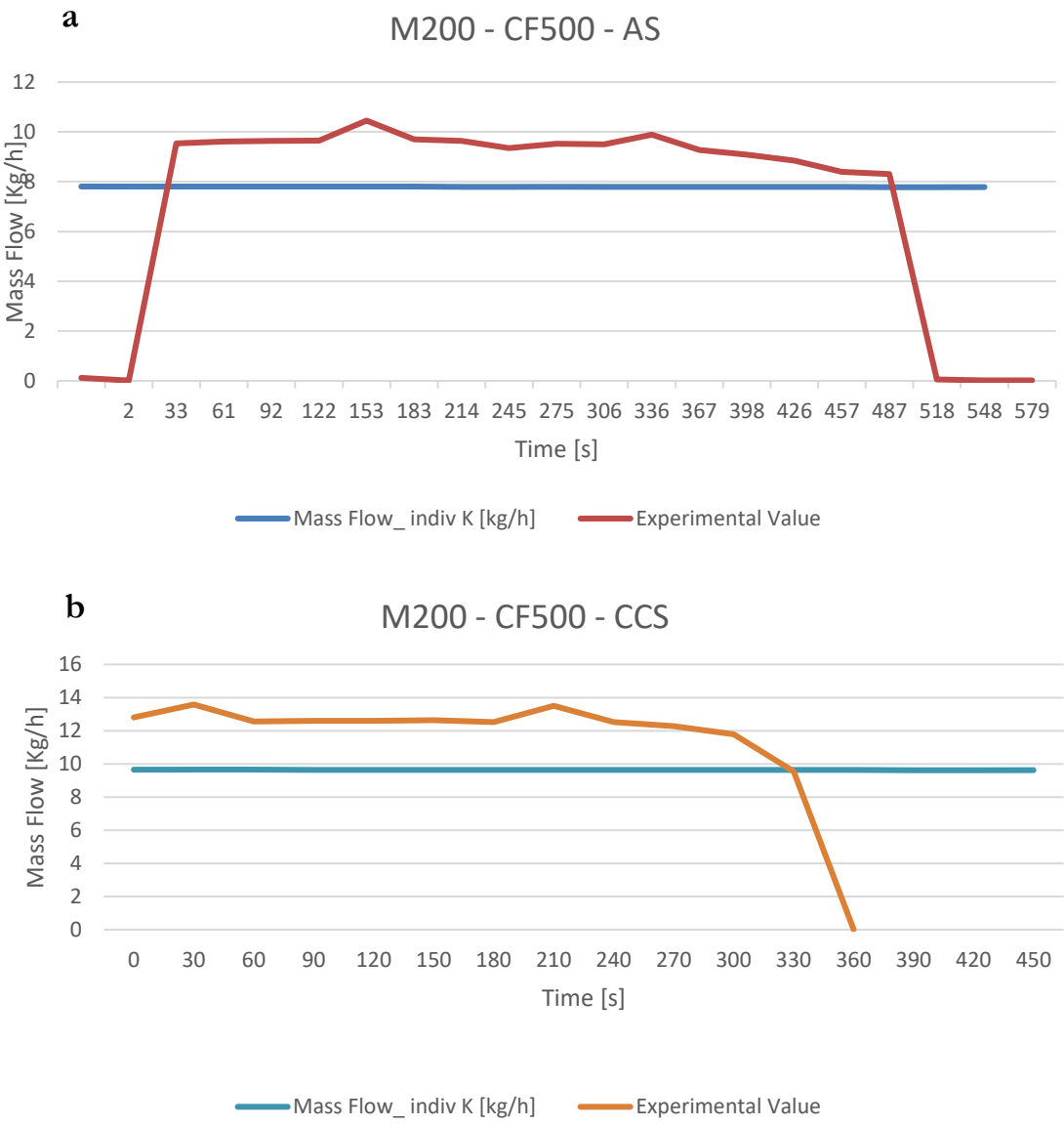

Figure 42: Mass flow experimental and predicted values comparison for the M200 together with CF500 and (a) AS and (b) CCS.

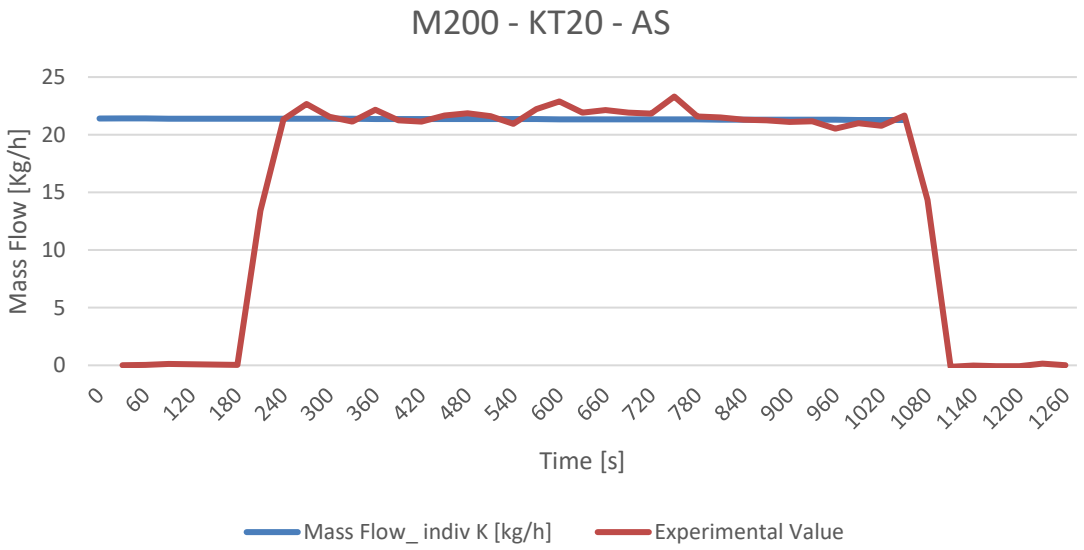

Figure 43: Mass flow experimental and predicted values comparison for the M200 together with KT20 and AS.

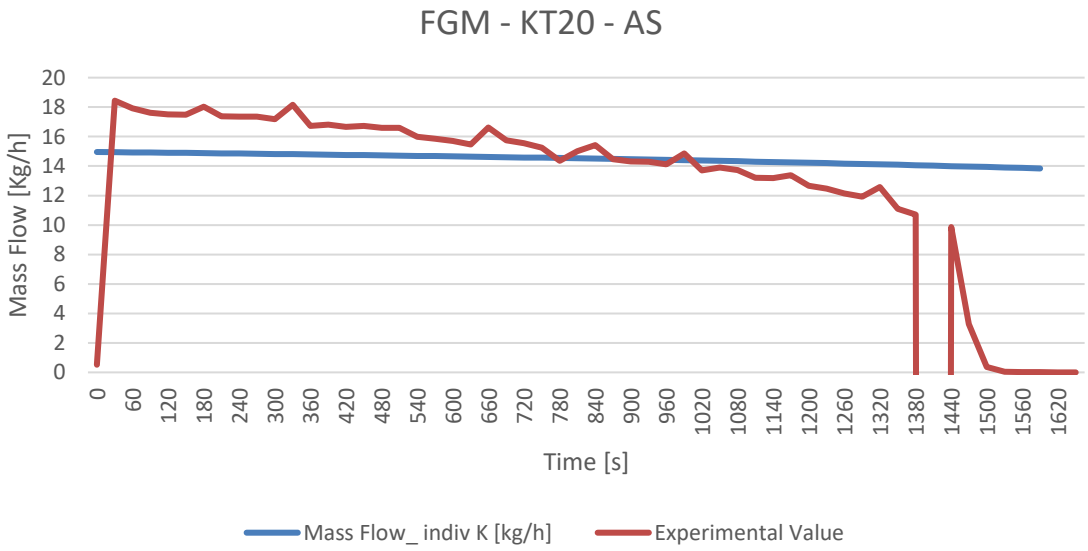

Figure 44: Mass flow experimental and predicted values comparison for the FGM together with KT20 and AS.

7.4.3 Mass flow predictions and experimental values comparison as group mass flow validation.

Table 7.7: Mass flow group predictions comparison to old experiments to 20% of screw speed

Feeder	Powder	Screw	Experimental mass flow	ffc group mass flow	Stat model group mass flow
CF0500_GB2	M100	AS'	2.998242	3.836057	3.836057
CF0500_GB2	M100	CCS'	3.919983	3.493737	3.493737
CF0500_GB2	M100	FCS'	1.845745	2.493144	2.407839
CF0500_GB2	PH102	AS'	1.613728	2.260708	1.605528
CF0500_GB2	PH102	CCS'	2.088274	2.058968	1.600151
CF0500_GB2	PH102	FCS'	0.958705	1.469287	0.658091
CF0500_GB2	PMIL	AS'	0.175729	0.331782	0.331782
CF0500_GB2	PMIL	CCS'	0.275669	0.060137	0.316847
CF0500_GB2	PMIL	FCS'	0.116974	0.072422	0.072422
CF0500_GB2_adh	PMIL	AS'	0.973989	0.331782	0.331782
CF0500_GB2_adh	PMIL	CCS'	1.113493	0.060137	0.316847
CF0500_GB2_adh	PMIL	FCS'	0.498739	0.072422	0.072422
K-CL-KT20	M100	AS'	5.899492	3.586403	3.586403
K-CL-KT20	M100	CCS'	5.368476	3.111225	3.111225
K-CL-KT20	M100	FCS'	2.465224	2.217517	2.141643
K-CL-KT20	PH102	AS'	4.327905	2.126956	1.510538
K-CL-KT20	PH102	CCS'	3.15526	1.845146	1.433977
K-CL-KT20	PH102	FCS'	1.37169	1.315123	0.589041
K-CL-KT20	PMIL	AS'	1.566642	0.322207	0.322207
K-CL-KT20	PMIL	CCS'	1.866369	0.055628	0.293088
K-CL-KT20	PMIL	FCS'	0.999463	0.066911	0.066911
MT-S Hyg	M100	CCS'	0.578777	0.433924	0.433924
MT-S Hyg	M100	FCS'	0.18519	0.117518	0.113497
MT-S Hyg	PH102	CCS'	0.398826	0.256378	0.199247
MT-S Hyg	PH102	FCS'	0.111141	0.069434	0.031099
MT-S Hyg	PMIL	CCS'	0.375852	0.007469	0.039353
ZD-12 FB	M100	CCS'	2.330649	1.881048	1.881048
ZD-12 FB	PH102	CCS'	1.856121	1.10798	0.86108

Table 7.8: Mass flow group predictions comparison to old experiments to 50% of screw speed

Feeder	Powder	Screw	Experimental mass flow	ffc group mass flow	Rev Stat group mass flow
CF0500_GB2	M100	AS'	7.533597	9.59014334	9.59014334
CF0500_GB2	M100	CCS'	9.306906	8.734343325	8.734343325
CF0500_GB2	M100	FCS'	4.949076	6.23285878	6.019597442
CF0500_GB2	PH102	AS'	3.889795	5.651769875	4.013819008
CF0500_GB2	PH102	CCS'	5.099759	5.147420298	4.000378368
CF0500_GB2	PH102	FCS'	2.390503	3.67321762	1.645227165

Feeder	Powder	Screw	Experimental mass flow	ffc group mass flow	Rev Stat group mass flow
CF0500_GB2	PMIL	AS'	0.680483	0.829456223	0.829456223
CF0500_GB2	PMIL	CCS'	0.831826	0.150342765	0.792116723
CF0500_GB2	PMIL	FCS'	0.349056	0.181053903	0.181053903
CF0500_GB2_adh	PMIL	AS'	1.943545	0.829456223	0.829456223
CF0500_GB2_adh	PMIL	CCS'	1.329738	0.150342765	0.792116723
CF0500_GB2_adh	PMIL	FCS'	0.862758	0.181053903	0.181053903
K-CL-KT20	M100	AS'	14.34763	8.966007979	8.966007979
K-CL-KT20	M100	CCS'	13.3468	7.778061896	7.778061896
K-CL-KT20	M100	FCS'	6.085098	5.543792373	5.354107893
K-CL-KT20	PH102	AS'	10.03372	5.317389285	3.776345933
K-CL-KT20	PH102	CCS'	7.372935	4.612864843	3.584942295
K-CL-KT20	PH102	FCS'	3.166601	3.287806818	1.472602402
K-CL-KT20	PMIL	AS'	3.894661	0.805517458	0.805517458
K-CL-KT20	PMIL	CCS'	4.490664	0.139069257	0.732719556
K-CL-KT20	PMIL	FCS'	2.224842	0.167276535	0.167276535
MT-S Hyg	M100	CCS'	1.380058	1.084810071	1.084810071
MT-S Hyg	M100	FCS'	0.497545	0.293794187	0.283741826
MT-S Hyg	PH102	CCS'	0.931004	0.64094593	0.498118686
MT-S Hyg	PH102	FCS'	0.272532	0.173584476	0.077748156
MT-S Hyg	PMIL	CCS'	0.0538	0.018672783	0.098382014
ZD-12 FB	M100	CCS'	5.919904	4.70262043	4.70262043
ZD-12 FB	PH102	CCS'	4.782036	2.76995099	2.152700067

Table 7.9: Mass flow group predictions comparison to old experiments to 80% of screw speed

Feeder	Powder	Screw	Experimental mass flow	ffc group mass flow	Rev Stat group mass flow
CF0500_GB2	M100	AS'	11.89909	15.34422934	15.34423
CF0500_GB2	M100	CCS'	14.27776	13.97494932	13.97495
CF0500_GB2	M100	FCS'	7.605163	9.972574048	9.631356
CF0500_GB2	PH102	AS'	5.971317	9.0428318	6.42211
CF0500_GB2	PH102	CCS'	7.915635	8.235872477	6.400605
CF0500_GB2	PH102	FCS'	3.711187	5.877148191	2.632363
CF0500_GB2	PMIL	AS'	1.37727	1.327129957	1.32713
CF0500_GB2	PMIL	CCS'	1.828042	0.240548424	1.267387
CF0500_GB2	PMIL	FCS'	1.013562	0.289686244	0.289686
CF0500_GB2_adh	PMIL	AS'	2.921655	1.327129957	1.32713
CF0500_GB2_adh	PMIL	CCS'	2.694819	0.240548424	1.267387
CF0500_GB2_adh	PMIL	FCS'	1.248264	0.289686244	0.289686
K-CL-KT20	M100	AS'	23.43716	14.34561277	14.34561
K-CL-KT20	M100	CCS'	21.57466	12.44489903	12.4449
K-CL-KT20	M100	FCS'	9.814798	8.870067796	8.566573
K-CL-KT20	PH102	AS'	15.09806	8.507822857	6.042153
K-CL-KT20	PH102	CCS'	11.16717	7.380583749	5.735908

Feeder	Powder	Screw	Experimental mass flow	ffc group mass flow	Rev Stat group mass flow
K-CL-KT20	PH102	FCS'	4.513187	5.260490909	2.356164
K-CL-KT20	PMIL	AS'	6.201715	1.288827933	1.288828
K-CL-KT20	PMIL	CCS'	4.820045	0.222510811	1.172351
K-CL-KT20	PMIL	FCS'	3.140199	0.267642457	0.267642
MT-S Hyg	M100	CCS'	2.246935	1.735696114	1.735696
MT-S Hyg	M100	FCS'	0.84087	0.470070698	0.453987
MT-S Hyg	PH102	CCS'	1.364978	1.025513488	0.79699
MT-S Hyg	PH102	FCS'	0.420557	0.277735162	0.124397
MT-S Hyg	PMIL	CCS'	0.072037	0.029876453	0.157411
ZD-12 FB	M100	CCS'	9.692341	7.524192688	7.524193
ZD-12 FB	PH102	CCS'	7.83149	4.431921583	3.44432

8 Literature

[1] Rathore A S and Winkle H 2009 Quality by design for biopharmaceuticals *Nat. Am.***27**

[2] Kaufman B and Novack G D 2003 Compliance issues in manufacturing of drugs *Ocul. Surf.***1** 80–5

[3] Moghtadernejad S, Escotet-Espinoza M S, Oka S, Singh R, Liu Z, Román-Ospino A D, Li T, Razavi S, Panikar S, Scicolone J, Callegari G, Hausner D and Muzzio F 2018 A Training on: Continuous Manufacturing (Direct Compaction) of Solid Dose Pharmaceutical Products *J. Pharm. Innov.***13** 155–87

[4] Yu L X 2008 Pharmaceutical quality by design: Product and process development, understanding, and control *Pharm. Res.***25** 781–91

[5] Engisch W E and Muzzio F J 2014 Loss-in-Weight Feeding Trials Case Study: Pharmaceutical Formulation *J. Pharm. Innov.***10** 56–75

[6] Rantanen J and Khinast J 2015 The Future of Pharmaceutical Manufacturing Sciences *J. Pharm. Sci.***104** 3612–38

[7] Allison G, Cain Y T, Cooney C, Garcia T, Bizjak T G, Holte O, Jagota N, Komas B, Korakianiti E, Kourti D, Madurawe R, Morefield E, Montgomery F, Nasr M, Randolph W, Robert J L, Rudd D and Zezza D 2015 Regulatory and quality considerations for continuous manufacturing May 20-21, 2014 continuous manufacturing symposium *J. Pharm. Sci.***104** 803–12

[8] Poechlauer P, Manley J, Broxterman R, Gregertsen B and Ridemark M 2012 Continuous processing in the manufacture of active pharmaceutical ingredients and finished dosage forms: An industry perspective *Org. Process Res. Dev.***16** 1586–90

[9] Byrn S, Futran M, Thomas H, Jayjock E, Maron N, Meyer R F, Myerson A S, Thien M P and Trout B L 2015 Achieving Continuous Manufacturing for Final Dosage Formation: Challenges and How to Meet Them. May 20-21, 2014 Continuous Symposium *J. Pharm. Sci.***104** 792–802

[10] Yu L X 2008 Pharmaceutical Quality by Design : Product and Process Development , Understanding , and Control **25**

[11] Bostijn N, Dhondt J, Ryckaert A, Szabó E, Dhondt W, Van Snick B, Vanhoorne V, Vervaet C and De Beer T 2019 A multivariate approach to predict the volumetric and gravimetric feeding behavior of a low feed rate feeder based on raw material properties *Int. J. Pharm.***557** 342–53

[12] Nowak S 2017 Three ways to improve continous loss-in-weight feeding accuracy

[13] Engisch W E and Muzzio F J 2015 Feedrate deviations caused by hopper refill of loss-in-

weight feeders *Powder Technol.***283** 389–400

[14] Mehos G *Hopper Design Principles for Chemical Engineers*

[15] Freeman T, Brockbank K and Armstrong B 2015 Measurement and quantification of caking in powders *Procedia Eng.***102** 35–44

[16] Hainz P 2019 *Understanding tribocharging effects during twin-screw feeding*

[17] Fernandez J W, Cleary P W and Mcbride W 2009 EFFECT OF SCREW DESIGN ON HOPPER DRAW DOWN BY A HORIZONTAL SCREW FEEDER 1–6

[18] Orefice L and Khinast J G 2017 DEM study of granular transport in partially filled horizontal screw conveyors *Powder Technol.***305** 347–56

[19] Roberts A W 1999 The influence of granular vortex motion on the volumetric performance of enclosed screw conveyors 56–67

[20] Coperion 2020 Designer Features

[21] Engisch W E and Muzzio F J 2012 Method for characterization of loss-in-weight feeder equipment *Powder Technol.***228** 395–403

[22] Vetter G 1998 *Dosing Handbook* ed E Science

[23] Wang Z, Escotet-Espinoza M S and Ierapetritou M 2017 Process analysis and optimization of continuous pharmaceutical manufacturing using flowsheet models *Comput. Chem. Eng.***107** 77–91

[24] Orefice L 2020 Discrete Elements Method modelling of screw conveying and related processes

[25] Van Snick B, Dhondt J, Pandelaere K, Bertels J, Mertens R, Klingeleers D, Di Pretoro G, Remon J P, Vervaet C, De Beer T and Vanhoorne V 2018 A multivariate raw material property database to facilitate drug product development and enable in-silico design of pharmaceutical dry powder processes *Int. J. Pharm.***549** 415–35

[26] Abdullah E C and Geldart D 1999 The use of bulk density measurements as flowability indicators

[27] Moondra S, Maheshwari R, Taneja N, Tekade M and Tekadle R K 2018 *Bulk Level Properties and its Role in Formulation Development and Processing* vol 2 (Elsevier Inc.)

[28] Martin Rhodes 2008 *Introduction to particle technology*

[29] Divya S and Ganesh G 2019 Characterization of powder flowability using FT4 - Powder rheometer *J. Pharm. Sci. Res.***11** 25–9

[30] Hancock B C 2019 The Wall Friction Properties of Pharmaceutical Powders, Blends, and Granulations *J. Pharm. Sci.***108** 457–63

[31] Arnold P C and Kadeen A S 1977 Reducing Hopper Wall Friction by Mechauical Vibration

*Powder Technol.***2** 6–9

[32] Thoorens G, Krier F, Leclercq B, Carlin B and Evrard B 2014 Microcrystalline cellulose, a direct compression binder in a quality by design environment - A review *Int. J. Pharm.***473** 64–72

[33] Horio T, Yasuda M and Matsusaka S 2014 Effect of particle shape on powder fl owability of microcrystalline cellulose as determined using the vibration shear tube method *Elsevier B.V.***473** 572–8

[34] McCrae J C, Morrison E E, MacIntyre I M, Dear J W and Webb D J 2018 Long-term adverse effects of paracetamol – a review *Br. J. Clin. Pharmacol.***84** 2218–30

[35] Joshi J T 2011 A Review on Micronization Techniques *J. Pharm. Sci. Technol.***3** 651–81

[36] Li J and Wu Y 2014 Lubricants in pharmaceutical solid dosage forms *Lubricants***2** 21–43

[37] Su W, Jia N, Li H, Hao H and Li C 2017 Polymorphism of D-mannitol: Crystal structure and the crystal growth mechanism *Chinese J. Chem. Eng.***25** 358–62